

An Ab Initio/Transition State Theory Study of the Reactions of \dot{C}_5H_9 Species of Relevance to 1,3-Pentadiene, Part II: Pressure Dependent Rate Constants and Implications for Combustion Modelling

Yanjin Sun¹, Chong-Wen Zhou^{1,2*}, Kieran P. Somers¹, Henry J. Curran^{1*}

¹Combustion Chemistry Centre, National University of Ireland, Galway, Ireland

²School of Energy and Power Engineering, Beihang University, Beijing 100191, P. R. China.

Abstract

The temperature- and pressure-dependence of rate constants for several radical and unsaturated hydrocarbon reactions ($1,3-C_5H_8/1,4-C_5H_8/cyC_5H_8 + \dot{H}$, $C_2H_4 + \dot{C}_3H_5-a$, $C_3H_6 + \dot{C}_2H_3$) are analysed in this paper. The abstraction reactions of these systems are also calculated and compared with available literature data. \dot{C}_5H_9 radicals can be produced via \dot{H} atom addition reactions to the pentadiene isomers and cyclopentene, and also by H-atom abstraction reactions from 1- and 2-pentene and cyclopentane. Comprehensive \dot{C}_5H_9 potential energy surface (PES) analyses and high-pressure limiting rate constants for related reactions have been explored in Part I of this work (*J. Phys. Chem. A* 2019, 123(22), 9019–9052). In this work, a chemical kinetic model is constructed based on the computed thermochemistry and high-pressure limiting rate constants from Part I, to further understand the chemistry of different C_5H_8 molecules. The most important channels for these addition reactions are discussed in the present work based on reaction pathway analyses. The dominant reaction pathways for these five systems are combined together to generate a simplified \dot{C}_5H_9 PES including nine reactants, 25 transition states (TSs) and nine products. Spin-restricted single point energies are calculated for radicals and TSs on the simplified PES at the ROCCSD(T)/aug-cc-pVTZ level of theory with basis set corrections from MP2/aug-cc-pVXZ (where $X = T$ and Q). Temperature- and pressure-dependent rate constants are calculated using RRKM theory with a Master Equation analysis, with restricted energies used for minima on the simplified \dot{C}_5H_9 PES and unrestricted energies for other species, over a temperature range of 300–2000 K and in the pressure range 0.01–100 atm. The rate constants calculated are in good agreement with the ones in the literature. The chemical kinetic model is updated with pressure-dependent rate constants and is used to simulate the species concentration profiles for \dot{H} atom addition to cyclopentane and cyclopentene. Through detailed analyses and comparison, this model can reproduce the experimental measurements of species qualitatively and quantitatively with reasonably good agreement.

■ Introduction

As highlighted in Part I of this study¹, olefins and dienes are important intermediates generated via heavy petroleum cracking. The reactions of \dot{C}_5H_9 radicals have an important effect on the performance of a C_5 combustion mechanism and may also influence the combustion chemistry of larger dienes and alkenes. \dot{H} atom addition to the pentadiene isomers and cyclopentene, allyl radical addition to ethylene, vinyl radical addition to propene, and H-atom abstraction reactions are all studied in this work. In Part I, high-level ab initio calculations were carried out to investigate the comprehensive \dot{C}_5H_9 PES upon \dot{H} atom addition to, and H-atom abstraction by \dot{H} atoms from 1,3-pentadiene. Thermochemistry for C_5 species involved in the \dot{C}_5H_9 PES have also been calculated using the MESS²⁻³ (Master Equation System Solver) code and compared with literature data resulting in very good agreement.

Here we present an investigation of temperature- and pressure-dependent rate constants using RRKM theory with Master Equation analysis. The aim of this work is to develop comprehensive kinetics for the title reaction for use in a detailed chemical kinetic model describing C_5 species oxidation. \dot{H} atom addition reactions to pentadiene isomers and cyclopentene have been extensively studied theoretically and literature papers describing the \dot{C}_5H_9 PES have been documented in Part I of this study.¹ Moreover, the thermochemistry of the C_5 species used in this study has been comprehensively validated against literature data in Part I. Here the important literature papers with kinetic calculations/estimations, and/or experimental measurements are discussed and synthesised in Table 1.

Table 1. Summary of the theoretical and experimental literature studies relevant to \dot{C}_5H_9 species

Year	Author	Reactions	T / K	p	Method	Result
Theoretical studies						
1991	W. Tsang ⁴	$\dot{C}_2H_3 + C_3H_6 \rightarrow C_2H_4 + \dot{C}_3H_5\text{-a}$ (1) $\dot{C}_2H_3 + C_3H_6 \rightarrow 1,3\text{-}C_4H_6 + \dot{C}H_3$ (2) $\dot{C}_2H_3 + C_3H_6 \rightarrow 1,3\text{-}C_5H_8 + \dot{H}$ (3)	–	–	$k(R1)$ analogy to abstraction of C_3H_6 by $\dot{C}H_3$. $k(R2)$ & $k(R3)$ estimated from Fahr and Stein's low-pressure pyrolysis reactor experiment ⁵ for \dot{C}_2H_3 addition to C_2H_4 and C_2H_2 .	k_∞
2003	Matheu et al. ⁶	$C_2H_4 + \dot{C}_3H_5\text{-a} \rightarrow 1,5\text{-}\dot{C}_5H_9$ $cyC_5H_8 + \dot{H} \rightarrow cy\dot{C}_5H_9$	–	High-pressure limiting (HPL)	CBS-Q	k_∞
2004	Saeys et al. ⁷	$C_2H_4 + \dot{C}_3H_5\text{-a} \leftrightarrow 1,5\text{-}\dot{C}_5H_9$ $1,3\text{-}C_4H_6 + \dot{C}H_3 \leftrightarrow 1,3\text{-}\dot{C}_5H_9$ $1,3\text{-}C_4H_6 + \dot{C}H_3 \leftrightarrow 3Me\text{-}1,4\text{-}\dot{C}_4H_6^a$	0, 298, 1000	–	CBS-QB3	E_a
2006	W. Tsang ⁸	Decomposition of 1,3- \dot{C}_5H_9 , 1,4- \dot{C}_5H_9 , 1,5- \dot{C}_5H_9	–	0.1, 1, 10 atm and HPL	Literature review and estimations	E_a, k_∞ and $k(T, p)$
2008	Sabbe et al. ⁹	$1,3\text{-}\dot{C}_5H_9 \leftrightarrow 1,3\text{-}C_4H_6 + \dot{C}H_3$ $C_2H_4 + \dot{C}_3H_5\text{-a} \leftrightarrow 1,5\text{-}\dot{C}_5H_9$	300–1300	HPL	CBS-QB3//B3LYP/6-311G(d,p)	E_a, k_∞
2008	Sirjean et al. ¹⁰	$cyC_5H_9 \leftrightarrow 1,5\text{-}\dot{C}_5H_9$ $cy\dot{C}_5H_9 \rightarrow cyC_5H_8 + \dot{H}$	500–2000	HPL	CBS-QB3//B3LYP/cbsb7	E_a, k_∞

2009	Goldsmith et al. ¹¹	$\dot{\text{C}}_2\text{H}_3 + \text{C}_3\text{H}_6$	300–2000	1, 15, 100 and 1000 Torr	G3 (B3PW91/6-31+G(d,p) for hindered-rotor treatment); Variflex with RRKM/ME theory	<ul style="list-style-type: none"> $\dot{\text{C}}_5\text{H}_9$ PES with 15 species and 48 TSs $k(T, p)$
2011	Awan et al. ¹²	$\text{cyC}_5\text{H}_8 + \dot{\text{H}} \leftrightarrow \text{cy}\dot{\text{C}}_5\text{H}_9$ $\text{cyC}_5\text{H}_9 \leftrightarrow 1,5\text{-}\dot{\text{C}}_5\text{H}_9$	700–1900	HPL	G3MP2B2	k_∞
2015	Wang et al. ¹³⁻¹⁴	$\text{C}_2\text{H}_4 + \dot{\text{C}}_3\text{H}_5\text{-a}$	500–1800	1 atm, HPL	ΔH_{rxn} from CBS-QB3 and/or rate rules; $k(T, p)$ calculated by QRRK theory.	<ul style="list-style-type: none"> $\dot{\text{C}}_5\text{H}_9$ PES with 20 species and 24 TSs k_∞ for 12 reactions and $k(T, p)$
2017	Al Rashidi et al. ¹⁵	$\text{cy}\dot{\text{C}}_5\text{H}_9 \rightarrow \text{cyC}_5\text{H}_8 + \dot{\text{H}}$ $\text{cyC}_5\text{H}_9 \rightarrow 1,5\text{-}\dot{\text{C}}_5\text{H}_9$	300–1200	HPL	UCCSD(T)-F12b/cc-pVTZ-F12 //M06-2X/6-311++G(d,p)	k_∞ calculated and $k(T, p)$ estimated based on the falloff parameters in Wang's study ¹³
2018	Manion and Awan ¹⁶	$\text{cyC}_5\text{H}_8 + \dot{\text{H}} \leftrightarrow \text{cy}\dot{\text{C}}_5\text{H}_9$ $\text{cyC}_5\text{H}_9 \leftrightarrow 1,5\text{-}\dot{\text{C}}_5\text{H}_9$ $\text{C}_2\text{H}_4 + \dot{\text{C}}_3\text{H}_5\text{-a} \leftrightarrow 1,5\text{-}\dot{\text{C}}_5\text{H}_9$	300–2000	HPL	G3MP2B2	k_∞
Experimental studies						
1965	Gordon et al. ¹⁷	$\text{cyC}_5\text{H}_9 \rightarrow \text{C}_2\text{H}_4 + \dot{\text{C}}_3\text{H}_5\text{-a}$	573–748	0.05–0.06 atm	Cylindrical quartz reaction cell set	$k(\text{cy}\dot{\text{C}}_5\text{H}_9 \rightarrow 1,5\text{-}\dot{\text{C}}_5\text{H}_9)$
1967	Getty et al. ¹⁸	$\dot{\text{C}}_2\text{H}_5 + \text{C}_3\text{H}_4\text{-a}$	374–471	–	Cylindrical quartz vessel, medium-pressure mercury arc (photolysis of aldehydes to generate $\dot{\text{R}}$)	$k(\dot{\text{C}}_2\text{H}_5 + \text{C}_3\text{H}_4\text{-a})$
1972	Watkins and Olsen ¹⁹	$\text{C}_2\text{H}_2 + \dot{\text{C}}_3\text{H}_7$	319–405	90–480 Torr	Photolysis of the n-C ₃ H ₈ /C ₂ H ₂ mixture and measured by gas	$k(\text{C}_2\text{H}_2 + \dot{\text{C}}_3\text{H}_7)$

					chromatography	
1975	Stein and Rabinovitch ²⁰	Decomposition of $\text{cy}\dot{\text{C}}_5\text{H}_9$ (generated by $\text{cyC}_5\text{H}_8 + \dot{\text{H}}$)	300	1 atm	Conventional high vacuum Pyrex system	E_a
1981	Baldwin and Walker ²¹	Oxidation of $\text{C}_2\text{-C}_5$ alkenes in H_2/O_2 mixtures	753–773	0.66 atm	Adding $\text{C}_2\text{-C}_5$ alkenes to H_2/O_2 mixtures in aged boric-acid-coated vessels	$k_{753\text{K}}(\text{1,3-}\dot{\text{C}}_5\text{H}_9 \leftrightarrow \text{1,3-C}_4\text{H}_6 + \dot{\text{C}}\text{H}_3)$ estimated
1986	Gierczak et al. ²²	$\text{cyC}_5\text{H}_9 \leftrightarrow \text{1,5-}\dot{\text{C}}_5\text{H}_9$	298.15	7.6–383.2 Torr	Photolysis of $\text{H}_2\text{S-cyC}_5\text{H}_8$ and $\text{H}_2\text{S-1,4-C}_5\text{H}_8$ mixtures	E_a
1986	Kopinke et al. ²³	Pyrolysis of 1-pentene (isotope labelled C=CCCC^{14})	873	1.5–2 atm	Stainless steel reactor	The production ratio for 1,3-butadiene with/without labelled C-atoms (78 : 22 labelled)
1988	Perrin et al. ²⁴	Isomerization of 1- and 2-pentene	743–772	10–100 Torr	Conventional static reaction vessel with H_2S -promoted	$k_{753\text{K}}(\text{1,3-}\dot{\text{C}}_5\text{H}_9 \leftrightarrow \text{1,3-C}_4\text{H}_6 + \dot{\text{C}}\text{H}_3)$
1992	W. Tsang ²⁵	Pyrolysis of 1,7- C_8H_{14} in Ar	1040–1200	2–7 atm	Single-pulse shock tube (ST)	<ul style="list-style-type: none"> Product distributions relative to the initial reactant concentration $k(\text{1,5-}\dot{\text{C}}_5\text{H}_9 \rightarrow \text{cyC}_5\text{H}_8 + \dot{\text{H}})/k(\text{1,5-}\dot{\text{C}}_5\text{H}_9 \rightarrow \text{C}_2\text{H}_4 + \dot{\text{C}}_3\text{H}_5\text{-a})$ ratio derived based on the measured $[\text{cyC}_5\text{H}_8]/[\text{C}_2\text{H}_4]$ ratio
1995	Handford-Styring and Walker ²⁶	Oxidation of cyC_5H_8 by adding cyC_5H_8 to $\text{H}_2\text{-O}_2$ mixtures	580–783	0.66 atm	Cylindrical Pyrex vessel with chromatography/mass spectrometry	$k(\text{cy}\dot{\text{C}}_5\text{H}_9 \rightarrow \text{1,5-}\dot{\text{C}}_5\text{H}_9)$
2000	Clarke et al. ²⁷	$\dot{\text{H}}$ + alkenes and haloalkenes	298–370	0.067 atm	High-pressure flow system	$k(\text{cyC}_5\text{H}_8 + \dot{\text{H}} \rightarrow \text{cy}\dot{\text{C}}_5\text{H}_9)$
2009	Goldsmith et	$\dot{\text{C}}_2\text{H}_3 + \text{C}_3\text{H}_6$	300–700	15, 25 and	Flow reactor + time-resolved absorption	The decay rate of $\dot{\text{C}}_2\text{H}_3$ was derived based on the measured

	al. ¹¹			100 Torr	spectroscopy	[C3H6].
2011	Awan et al. ¹²	Decomposition of cy \dot{C}_5H_9 (generated by cyC ₅ H ₁₀ + \dot{H})	950–1116	2.3–3.4 atm	ST	<ul style="list-style-type: none"> Product concentrations $k(1,5-\dot{C}_5H_9 \rightarrow C_2H_4 + C_3H_5-$ a) derived from [C₂H₄]/[cyC₅H₈] ratio at 0.1–1000 bar and 700–1900 K
2017	Al Rashidi et al. ¹⁵	Decomposition of cyC ₅ H ₁₀ (cyC ₅ H ₁₀ /O ₂ /N ₂ mixture)	740–1250	10 atm ($\phi = 0.5$ – 3.0)	Jet stirred reactor (JSR)	<ul style="list-style-type: none"> Reactants and products concentrations
2018	Manion and Awan ¹⁶	Decomposition of cy \dot{C}_5H_9 (generated by cyC ₅ H ₈ + \dot{H})	863–1167	1.6–3.7 atm	ST	<ul style="list-style-type: none"> Reactant and product concentrations $k(1,5-\dot{C}_5H_9 \rightarrow C_2H_4 + C_3H_5-$ a) and $k_{\infty}(cyC_5H_8 + \dot{H} \leftrightarrow cy\dot{C}_5H_9)$ derived from [C₂H₄]/[cyC₅H₈] ratio at experimental condition

^a 3Me-1,4- \dot{C}_4H_6 represents 3-methyl-1-buten-4-yl radical (W14 in this study).

Based on our literature review, several features of these studies are summarized. (1) Most of the previous theoretical studies focused on reactions of radical addition to alkenes and/or the related reactions of cyclopentyl radical; a systematic study of reactions on the \dot{C}_5H_9 PES only began with Goldsmith's work¹¹ in 2009. In previous studies, there have been, at most, 20 minima and 48 TSs explored on the \dot{C}_5H_9 PES. In addition, the electronic energies of species on the \dot{C}_5H_9 PES were studied at the CBS-QB3, G3 or similar levels of theory except for the work of Al Rashidi¹⁵ which only included high-level theory calculations for one reaction on the \dot{C}_5H_9 PES. (2) With the exception of four experimental studies ($740 < T < 1250$ K), all other experimental studies were performed at temperatures below 1000 K. Seven out of the fifteen experimental studies were carried out at pressures below 1 atm with the lowest pressure being 7.6 Torr. As shown in Table 1, there are no direct measurements of 1,3-pentadiene + \dot{H} and the existing experimental studies have mainly focused on the C_2/C_3 , 1-pentene, 2-pentene, cyclopentene and cyclopentane systems. Even though some of the important reactions on the \dot{C}_5H_9 PES have been studied both theoretically and experimentally, a more systematic study is needed at a high-level of theory, providing thermochemistry and kinetic properties over a wide-range of temperatures and pressures, especially from the perspective of \dot{H} atom addition to dienes (1,3-pentadiene, 1,4-pentadiene, etc.).

In Part I we illustrated the \dot{C}_5H_9 PES by discussing the reaction mechanism and kinetics of each \dot{C}_5H_9 radical. For any species on the \dot{C}_5H_9 PES, we are able to determine the detailed chemistry by tracing the first well (\dot{C}_5H_9 isomers) which is connected to the species. In addition, the high-pressure limiting rate constants which are calculated at the UOCCSD(T)/aug-cc-pVXZ level of theory ($X = T$ and Q) for 88 reactions on this PES are provided. For the 88 reactions studied (the forward and the reverse direction of a specific reaction is considered as one reaction), to the authors' knowledge, (1) high-pressure limiting rate constants for ~12 reactions are available in the literature over a wide range of temperature and pressure; (2) pressure-dependent rate constants are available for ~11 reactions; (3) enthalpy and entropy data are available for 8 of the 22 C_5 species and only 5 of them have existing heat capacities at temperatures in the range 300–1500 K. (4) ~12 reactions have been implemented in combustion models (e.g. AramcoMech3.0²⁸⁻³⁵ and Awan and Manion's work^{12, 16}).

In the current work, a chemical kinetic model describing the \dot{C}_5H_9 PES is firstly developed using the high-pressure limiting rate constants for \dot{H} atom addition reactions, H-atom abstraction reactions by \dot{H} atoms and other radicals, and unimolecular decomposition reactions of related species. Thereafter, rate of production (ROP) analyses were performed

using ANSYS Chemkin-Pro³⁶ to determine the important chemical pathways associated with 1,3-, 1,4-pentadiene, cyclopentene + $\dot{\text{H}}$, and vinyl + propene oxidation kinetics and a simplified $\dot{\text{C}}_5\text{H}_9$ PES was generated, containing the important reaction channels. The SPEs for minima on the simplified PES are re-calculated at the higher, ROCCSD(T)/aug-cc-pVXZ (where $X = \text{T}$ and Q), level of theory. Thereafter temperature- and pressure-dependent rate constants of reactions on the complete PES are calculated using MESS, with restricted energies used for species on the simplified $\dot{\text{C}}_5\text{H}_9$ PES and unrestricted energies for other species. Finally, a comprehensive model containing pressure-dependent rate constants with additional secondary chemistry (e.g. 1-, 2-pentene, cyclopentane, cyclopentene) was developed. This model has been used to simulate available literature data, with deviations of absolute species concentrations and product ratios of major products being within a factor of two of experimental measurements.

■ Computational methods

• Theoretical methods

Primary reactions

The theoretical methods used for quantum and thermochemistry calculations for reactions on the $\dot{\text{C}}_5\text{H}_9$ PES are described in detail in Part I,¹ and only the methods used to determine the minima on the simplified PES are described here. For free radicals with a single unpaired electron, the spin-unrestricted functions treat the variation of two sets of spatial molecular orbitals (ψ_i^α and ψ_i^β) as being completely independent in order to minimize the expectation value of the total energy.³⁷ However, the unrestricted wave functions are not Eigen functions of the spin-squared operators S^2 , and thus an unrestricted wave function for a radical with one unpaired electron contains significant contamination by components of higher multiplicity such as quartets.³⁸ To address this problem, a spin-restricted coupled-cluster (ROCCSD(T)) method³⁹ is used in the SPE calculations to reduce spin contamination in the correlated wave function. In this work, the important species and TSs for the 1,3-pentadiene + $\dot{\text{H}}$ system are identified using ROP simulations. Then, the spin-restricted SPEs for minima and TSs on the simplified $\dot{\text{C}}_5\text{H}_9$ PES are calculated using the same equation (Eq.1)⁴⁰⁻⁴¹ with spin-unrestricted SPE calculations which is described in Part I. The relative energies of spin-unrestricted and spin-restricted calculations are compared, resulting in a difference of less than 0.6 kcal mol⁻¹ for wells and varies from 0.2 to 1.4 kcal mol⁻¹ for TSs.

$$(1) \quad E_{\text{SPE}} = E_{\text{CCSD(T)/aug-cc-pVTZ}} + (E_{\text{MP2/aug-cc-pVQZ}} - E_{\text{MP2/aug-cc-pVTZ}})$$

The pressure-dependent rate constants are calculated using MESS which implements the one-dimensional Master Equation calculation for an arbitrary number of wells and products.² The single-exponential-down model $\langle \Delta E_d \rangle = 234(T/300)^{0.88} \text{ cm}^{-1}$ used to model energy transfer is selected based on previous ab initio studies concerning C₄ and C₅ hydrocarbons.⁴²⁻⁴³ Rashidi and co-workers used $\langle \Delta E_d \rangle = 200(T/300)^{0.80} \text{ cm}^{-1}$ for cyclopentyl + O₂,⁴² and Li and co-workers used $\langle \Delta E_d \rangle = 200(T/300)^{0.75} \text{ cm}^{-1}$ for C₄H₆ + H.⁴³ For the parameters in this model, it is commonly suggested that the power n be approximately 0.8; the $\Delta E_{\text{down}}^{(300)}$ ranges from 50–500 cm⁻¹ with larger species generally having higher values.⁴⁴ Thus the parameters in this paper are close to those used in the literature for C₄ and C₅ hydrocarbons with a slightly larger $\Delta E_{\text{down}}^{(300)}$.

The collision frequency used in the master equation simulation is estimated using the Lennard-Jones (L-J) parameters where ε is the well depth and σ is the characteristic distance.⁴⁵ In this study, the L-J parameters for C₅H₉ radicals are analogous to the parameters for C₅H₁₂ calculated by Jasper and Miller⁴⁶ from full-dimensional intermolecular potentials using several methods, $\sigma = 4.23 \text{ \AA}$, $\varepsilon = 192.0 \text{ cm}^{-1}$ for C₅H₉ radicals and $\sigma = 3.68 \text{ \AA}$, $\varepsilon = 67.89 \text{ cm}^{-1}$ for N₂⁴⁶ as the bath gas; $\sigma = 4.04 \text{ \AA}$, $\varepsilon = 235.0 \text{ cm}^{-1}$ for C₅H₉ radicals and $\sigma = 3.33 \text{ \AA}$, $\varepsilon = 94.87 \text{ cm}^{-1}$ for Ar⁴⁶ as the bath gas. To our knowledge, there are no high-level L-J parameters calculated for C₅H₁₀ and C₅H₉ in the literature. We have carried out MESS calculations of L-J parameters for C₅H₉ based on analogy with C₅H₁₀ ($\sigma = 5.49 \text{ \AA}$, $\varepsilon = 268.32 \text{ cm}^{-1}$ from AramcoMech 3.0). The maximum differences in the pressure-dependent rate constants observed were 20% at 1000 K, with no obvious differences at 2000 K. It should be noted that the L-J parameters for C₅H₁₂ calculated by Jasper and Miller are $\sigma = 4.23 \text{ \AA}$, $\varepsilon = 192.0 \text{ cm}^{-1}$ in comparison with $\sigma = 5.59 \text{ \AA}$, $\varepsilon = 272.14 \text{ cm}^{-1}$ employed in AramcoMech 3.0. Hence, more studies of transport parameters need to be performed to accurately predict pressure-dependent rate constants, especially for larger alkenes and dienes.

The low-frequency torsional modes are treated as one-dimensional hindered rotors ignoring the coupling between adjacent torsional modes, and the hindrance potentials as a function of dihedral angle are calculated at the M06-2X/6-311++G(d,p) level of theory. The hindrance potentials are fitted to Fourier series, and the molecular geometries of each species are used to estimate rotational constants. Once the potential is obtained, the energy levels for the rotation are determined by solving a 1-D Schrödinger equation.⁴⁷ The energy levels from this calculation are used to calculate the partition functions as a function of temperature by direct counting for each internal rotation. Quantum mechanical tunnelling corrections are

included for all TSs using an asymmetrical Eckart barrier model.⁴⁸ The temperature- and pressure-dependent rate constants calculated in this study are fitted to the modified Arrhenius expression as a function of temperature and provided as Supporting Information. Moreover, there are some global keywords in the MESS input file which can influence the calculation of rate constants (e.g. Method Parameters, Energy Grid Parameters). In this work, we have selected rational levels of theory for quantum calculations and carried out tests to carefully confirm the global keywords used in our rate constant calculations.

Secondary reactions

To understand the importance of $\dot{\text{H}}$ atom addition reactions at intermediate and high temperatures, the unimolecular decomposition reactions of 1,3-pentadiene and H-atom abstraction reactions of different reactants are calculated at lower levels of theory compared with $\dot{\text{H}}$ atom addition reactions. The geometries and frequencies for the unimolecular decomposition products are calculated at the $\omega\text{B97XD}/\text{aug-cc-pVTZ}$ level of theory, and the SPEs are calculated at the $\text{CCSD(T)}/\text{aug-cc-pVTZ}$ level of theory. The high-pressure limiting rate constants for the unimolecular decomposition reactions of 1,3-pentadiene are calculated based on the principle of microscopic reversibility (thermodynamic reversibility). This principle is widely used in kinetic modeling when the high-pressure limiting rate constants for a reaction of interest is unknown, and sensible rate constants for the reverse reaction can be inferred based on an analogy with a similar well-known chemical reaction.⁴⁹ Thereafter, pressure-dependent rate constants are calculated using Quantum-Rice-Ramsperger-Kassel (QRRK) theory with a Modified Strong Collision (MSC) approximation which is implemented in the ChemDis code.⁵⁰⁻⁵¹ For H-atom abstraction reactions from 1,3-, 1,4-pentadiene, cyclopentene and cyclopentene by $\dot{\text{H}}$ atoms, and H-atom abstraction reactions from propene by vinyl radicals, the quantum calculations are carried out at the $\text{CCSD(T)}/\text{aug-cc-pVTZ}//\omega\text{B97XD}/\text{aug-cc-pVTZ}$ level of theory with the basis set for SPE calculations corrected using the $\text{MP2}/\text{aug-cc-pVQZ}$ method, with the rate constants calculated using MESS.

- **Detailed kinetic modelling**

In this work, two chemical kinetic models were built. The first only consists of high-pressure limiting rate constants for $\dot{\text{H}}$ atom addition to 1,3-pentadiene reactions, H-atom abstraction reactions by $\dot{\text{H}}$ atoms from 1,3-, 1,4-pentadiene and cyclopentane, and unimolecular decomposition reaction of 1,3-pentadiene. The purpose of this is to identify the

important reactions on the \dot{C}_5H_9 PES for the 1,3-pentadiene + \dot{H} system. Thereafter, higher-level of theory SPE calculations can be applied to the important species and reactions. ANSYS Chemkin-Pro³⁶ is used to run ROP analyses which can provide complementary information on the direct contributions of individual reactions to species net production rates. The dilute mixture used for the ROP simulation is 0.0001% 1,3- C_5H_8 with 0.01% hydrogen atom in nitrogen at 1 atm and at different temperatures.

A more comprehensive model (the second model) was built by implementing our thermochemistry and kinetic results into AramcoMech 3.0,²⁸⁻³⁵ including higher-level RO-aug-cc-VXZ ($X = T$ and Q) SPE calculations for 18 minima and 25 reactions on a simplified \dot{C}_5H_9 PES. These 25 reactions are also proposed to be important for the combustion of 1- and 2-pentene, cyclopentene and cyclopentane as presented in Table 1 for previous experimental studies. Aiming to accurately simulate these experiments, rate constants for a series of secondary reactions have also been added to the mechanism, based on theoretical calculations, analogies to similar chemistry in AramcoMech 3.0, or from the literature. For experiments involving radical initiators and scavengers, the thermochemistry and kinetic parameters for these species have also been added to the mechanism to appropriately simulate the literature experiments. In previous experimental studies of cyclopentene + \dot{H} ¹⁶ and cyclopentane + \dot{H} ,¹² 1,3,5-trimethylbenzene (135TMB) was used as both a rate reference for \dot{H} atom reactions and as a radical scavenger. Hexamethylethane (HME) was used as a \dot{H} atom source for different mixtures at temperatures above 1000 K.

On the basis of the C_0 – C_4 combustion chemistry in AramcoMech 3.0, the major updates of the \dot{C}_5H_9 mechanism can be classified into five categories: (1) The calculated results from this work are updated, including thermochemistry data for C_5 species, pressure-dependent rate constants for reactions on the \dot{C}_5H_9 PES, H-atom abstraction reaction from 1,3-, 1,4-pentadiene, cyclopentene and cyclopentane by \dot{H} atoms, H-atom abstraction reaction from propene by vinyl radicals, and also the unimolecular decomposition of 1,3-pentadiene. (2) The related reactions for 1- and 2-pentene with hydrogen atoms and their kinetics and thermodynamics are taken from Power et al.;⁵² (3) The reactions related to the \dot{C}_4H_7 PES from the perspective of 1,3-butadiene + \dot{H} are updated from Li et al.;⁴³ (4) The thermochemistry and kinetic parameters for 135TMB, HME and their subsequent reactions are mainly from Power et al.,⁵² as 135TMB and HME have also been used in 1-, and 2-pentene + \dot{H} experiments by Awan et al.⁵³ as radical scavenger and a \dot{H} atom source. (5) The related reactions of cyclopentene/cyclopentane decomposition from Al Rashidi et al.^{15, 54} are also added. Thermochemical properties for these additional species are obtained from the

literature^{15, 54-55} and/or calculated using the group additivity method incorporated in the THERM code.⁵⁶

■ Results and discussion

• Reaction pathway analysis exploring the dominant channels

The first chemical kinetic model for the \dot{C}_5H_9 PES was built using high-pressure limiting rate constants for 88 reactions; including \dot{H} atom addition reactions, 14 reactions from H-atom abstraction by \dot{H} atoms and 7 unimolecular decomposition reactions. The PES for unimolecular decomposition reactions from 1,3-pentadiene and rate constant comparisons are described in detail in Figure S1. The thermochemical properties for C_5 species are calculated using MESS, while the thermochemistry for C_0 – C_4 species are adopted from AramcoMech 3.0. Since the unimolecular decomposition, H-atom abstraction by \dot{H} atoms and \dot{H} atom addition reactions to hydrocarbon fuels are important reaction classes at high temperatures, reaction pathway analyses are performed at 1400 K and 1800 K and 1 atm when 20% 1,3-pentadiene is consumed, as shown in Figures 1 and 2. The important channels are marked in red.

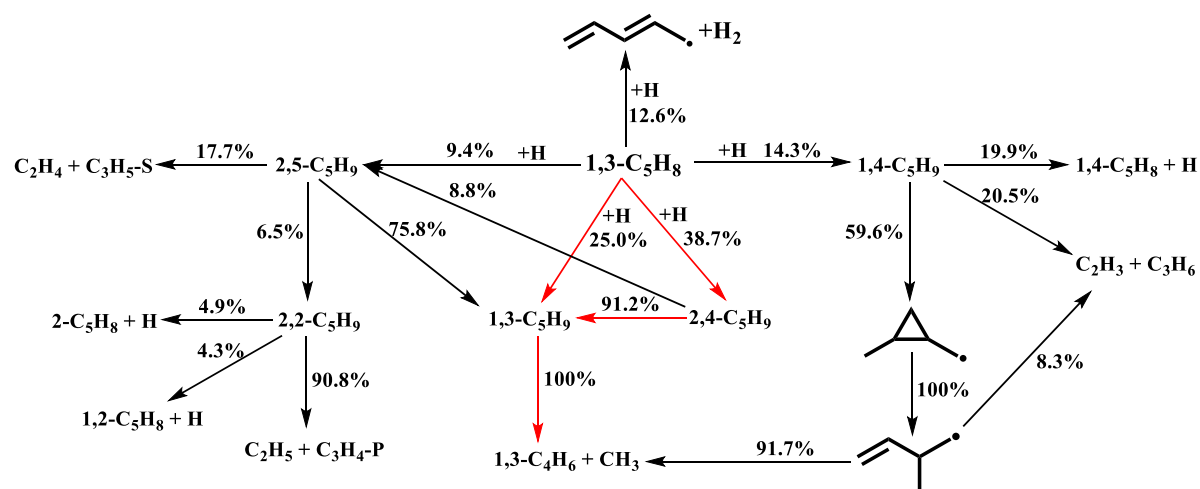


Figure 1. Flux analysis at 20% fuel consumption for 0.0001% 1,3-C₅H₈, 0.01% \dot{H} in N₂, $p = 1$ atm, $T = 1400$ K.

At 1400 K, the dominant consumption pathways are the formation of 2,4- \dot{C}_5H_9 (38.7%) and 1,3- \dot{C}_5H_9 (25.0%) radicals via \dot{H} atom addition reactions. Moreover, 91.2% of 2,4- \dot{C}_5H_9 radicals isomerize to 1,3- \dot{C}_5H_9 radicals. Thus, these two isomerisation reaction channels combined with the \dot{H} atom addition entrance channel result in 60.3% of the 1,3-pentadiene reactant producing 1,3- \dot{C}_5H_9 radicals, which undergo β -scission producing 1,3-butadiene + $\dot{C}H_3$ radicals. 14.3% of 1,3-C₅H₈ + \dot{H} forms 1,4- \dot{C}_5H_9 radicals which can undergo subsequent

exo-cyclisation, ring-opening and finally β -scission reactions to form 1,3-butadiene + $\dot{\text{C}}\text{H}_3$ radicals. In addition, 1,4- $\dot{\text{C}}_5\text{H}_9$ radicals can also undergo C–H β -scission to form 1,4-pentadiene + $\dot{\text{H}}$, or C–C β -scission to form vinyl + propene which can also be formed via β -scission of 3-methyl-1-buten-4-yl radicals (W14). 9.4% of the reaction flux produces 2,5- $\dot{\text{C}}_5\text{H}_9$ radicals. In addition, 8.8% of 2,4- $\dot{\text{C}}_5\text{H}_9$ radicals undergo isomerization reaction to also form 2,5- $\dot{\text{C}}_5\text{H}_9$ radicals. Subsequently, 75.8% of 2,5- $\dot{\text{C}}_5\text{H}_9$ radicals isomerize to 1,3- $\dot{\text{C}}_5\text{H}_9$ radicals, 6.5% isomerize to 2,2- $\dot{\text{C}}_5\text{H}_9$ radicals and 17.7% produce ethylene + 1-propenyl radical via β -scission reactions. 2,2- $\dot{\text{C}}_5\text{H}_9$ radicals mainly undergo β -scission reactions to form propyne + ethyl radical, and very small amount of 2-pentyne + $\dot{\text{H}}$ atom and 1,2-pentadiene + $\dot{\text{H}}$ atom. In addition, 12.6% of the reactant undergoes H-atom abstraction reactions by $\dot{\text{H}}$ atom to form 1,3-pentadien-5-yl radical + H_2 .

Figure 1 shows that at 1400 K the dominant products for the reaction between 1,3-pentadiene and $\dot{\text{H}}$ atoms are 1,3-butadiene + $\dot{\text{C}}\text{H}_3$ radical (75.2%), of which about 90% is produced from the β -scission reaction of 1,3- $\dot{\text{C}}_5\text{H}_9$ radicals. The other important products generated are 1,3-pentadien-5-yl radical + H_2 (12.6%), vinyl radical + propene (3.6%), 1,4-pentadiene + $\dot{\text{H}}$ atom (2.8%), ethylene + 1-propenyl radical (2.3%), propyne + ethyl radical (0.8%).

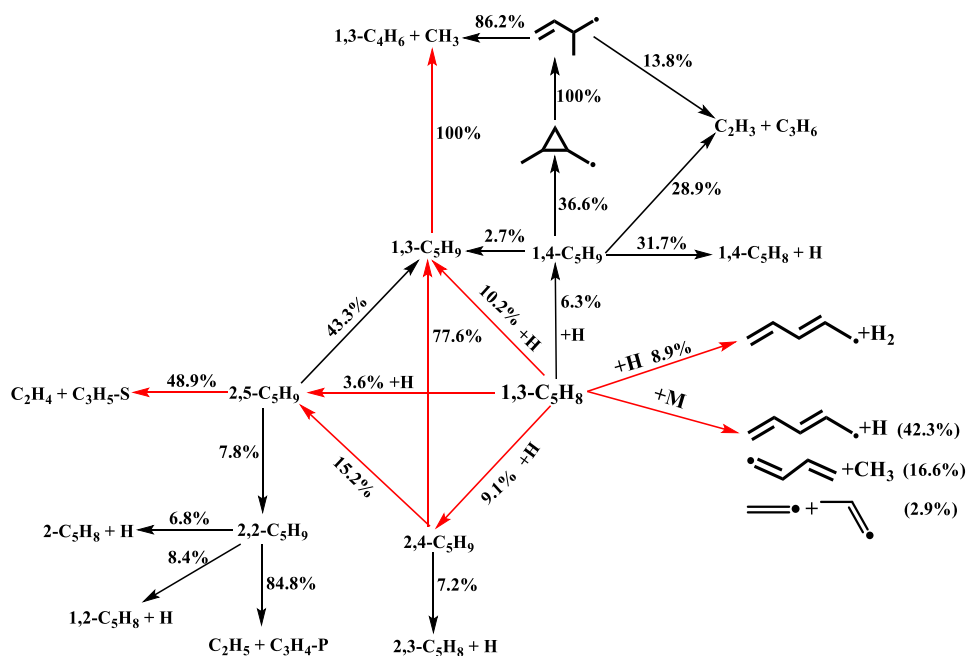


Figure 2. Flux analysis at 20% fuel consumption for 0.0001% 1,3- C_5H_8 , 0.01% $\dot{\text{H}}$ in N_2 , $p = 1$ atm, $T = 1800$ K.

At 1800 K, unimolecular decomposition reactions consume 61.8% of 1,3-pentadiene in total, of which 42.3% undergo C–H β -scission to produce 1,3-pentadien-5-yl radicals + $\dot{\text{H}}$

atoms and 16.6% produce 1,3-butadien-1-yl + $\dot{\text{C}}\text{H}_3$ radicals via C–C β -scission. A small amount of vinyl + 1-propenyl (2.9%) radical can also be formed via C–C β -scission reactions. Another 8.9% of 1,3-pentadiene is consumed by H-atom abstraction reactions by $\dot{\text{H}}$ atoms to produce 1,3-pentadien-5-yl radical + H_2 . The amount of reactant consumed via $\dot{\text{H}}$ atom addition reactions decreases from 87.4% at 1400 K to 29.3% at 1800 K. Among the four $\dot{\text{C}}_5\text{H}_9$ radicals formed via $\dot{\text{H}}$ atom addition reactions to 1,3-pentadiene, the most important is 1,3- $\dot{\text{C}}_5\text{H}_9$ which consumes 19.6% of the reactant with the contribution of direct $\dot{\text{H}}$ atom addition reaction (10.2%), isomerisation reaction from 2,4- $\dot{\text{C}}_5\text{H}_9$ (7.1%), and isomerisation reaction from 2,5- $\dot{\text{C}}_5\text{H}_9$ (2.2%). Thereafter 1,3- $\dot{\text{C}}_5\text{H}_9$ radicals undergo β -scission to form 1,3-butadiene + $\dot{\text{C}}\text{H}_3$ radicals which can also be formed in small amounts through β -scission of 3-methyl-1-buten-4-yl radicals (W14). Both 3-methyl-1-buten-4-yl and 1,4- $\dot{\text{C}}_5\text{H}_9$ radicals can produce vinyl radicals + propene via C–C β -scission, while 1,4- $\dot{\text{C}}_5\text{H}_9$ radicals can also undergo C–H β -scission to produce 1,4-pentadiene + $\dot{\text{H}}$ atoms. $\dot{\text{H}}$ atoms also consume 9.1% of 1,3-pentadiene forming 2,4- $\dot{\text{C}}_5\text{H}_9$ which mainly undergo isomerization reactions to form 1,3- $\dot{\text{C}}_5\text{H}_9$ and 2,5- $\dot{\text{C}}_5\text{H}_9$ radicals, the remaining 7.2% of 2,4- $\dot{\text{C}}_5\text{H}_9$ radicals produce 2,3-pentadiene + $\dot{\text{H}}$ atoms through a β -scission reaction. In addition, a small amount of 2,5- $\dot{\text{C}}_5\text{H}_9$ radicals can be formed through a $\dot{\text{H}}$ atom addition reaction and isomerization reaction of 2,4- $\dot{\text{C}}_5\text{H}_9$ radicals, then half of the radicals undergo β -scission to form ethylene + 1-propenyl radical, 43.3% isomerize to 1,3- $\dot{\text{C}}_5\text{H}_9$ radicals, and 7.8% isomerize to 2,2- $\dot{\text{C}}_5\text{H}_9$ radicals which mainly form propyne + ethyl radicals.

In general, the important products for 1,3-pentadiene + $\dot{\text{H}}$ at 1800 K are different from those at 1400 K. Although the unimolecular decomposition reactions start to play a major role and H-atom abstraction reactions become competitive with $\dot{\text{H}}$ atom additions, the reader should keep in mind that the current simulations are in an excess of H atom, and the relative ratios of unimolecular and bimolecular reaction will vary under different conditions. At 1800 K, 1,3-pentadiene reacts with $\dot{\text{H}}$ atoms to produce various products: 1,3-pentadien-5-yl radical + $\dot{\text{H}}$ (42.3%), 1,3-butadiene + $\dot{\text{C}}\text{H}_3$ radical (21.6%), 1,3-butadien-1-yl + $\dot{\text{C}}\text{H}_3$ radical (16.6%), 1,3-pentadien-5-yl radical + H_2 (8.9%), vinyl radical + 1-propenyl radical (2.9%), ethylene + 1-propenyl radical (2.4%), vinyl radical + propene (2.1%), 1,4-pentadiene + $\dot{\text{H}}$ atom (2.0%), 2,3-pentadiene + $\dot{\text{H}}$ atom (0.7%), propyne + ethyl radical (0.3%).

- **Simplified \dot{C}_5H_9 PES**

As outlined above, the important reaction channels for \dot{H} atom addition to 1,3-pentadiene were determined based on reaction pathway analyses. Similarly, the important reaction channels for 1,4- $C_5H_8 + \dot{H}$, $cyC_5H_8 + \dot{H}$ and $\dot{C}_2H_3 + C_3H_6$ have also been explored. These important reactions usually have lower barrier heights compared with the other channels starting from the same reactants or intermediates, which are consistent with our barrier height analyses presented in Part I. A simplified PES is generated containing the most important reaction channels for these systems and is shown in Figure 3, including nine wells, nine products and 25 TSs. The spin-restricted energies are calculated for radicals and TSs involved in these important reactions, the ZPVE corrected spin-restricted electronic energies for species on the simplified PES are shown in Table 2 and compared with ZPVE corrected spin-unrestricted energies. From the comparison, we can see that the spin-restricted energies are less than $0.6 \text{ kcal mol}^{-1}$ lower than spin-unrestricted energies for wells and radical products, but the differences for TSs can be up to $1.5 \text{ kcal mol}^{-1}$. In particular, the energy differences for TSs of the four entrance channels and the formation of 1,3-butadiene + $\dot{C}H_3$ are within $1\text{--}1.5 \text{ kcal mol}^{-1}$. Considering the trade-off between accuracy and computational cost, the spin-unrestricted SPE calculations are used for the full \dot{C}_5H_9 PES and the spin-restricted SPE calculations are only used for the species and TSs involved in important reactions.

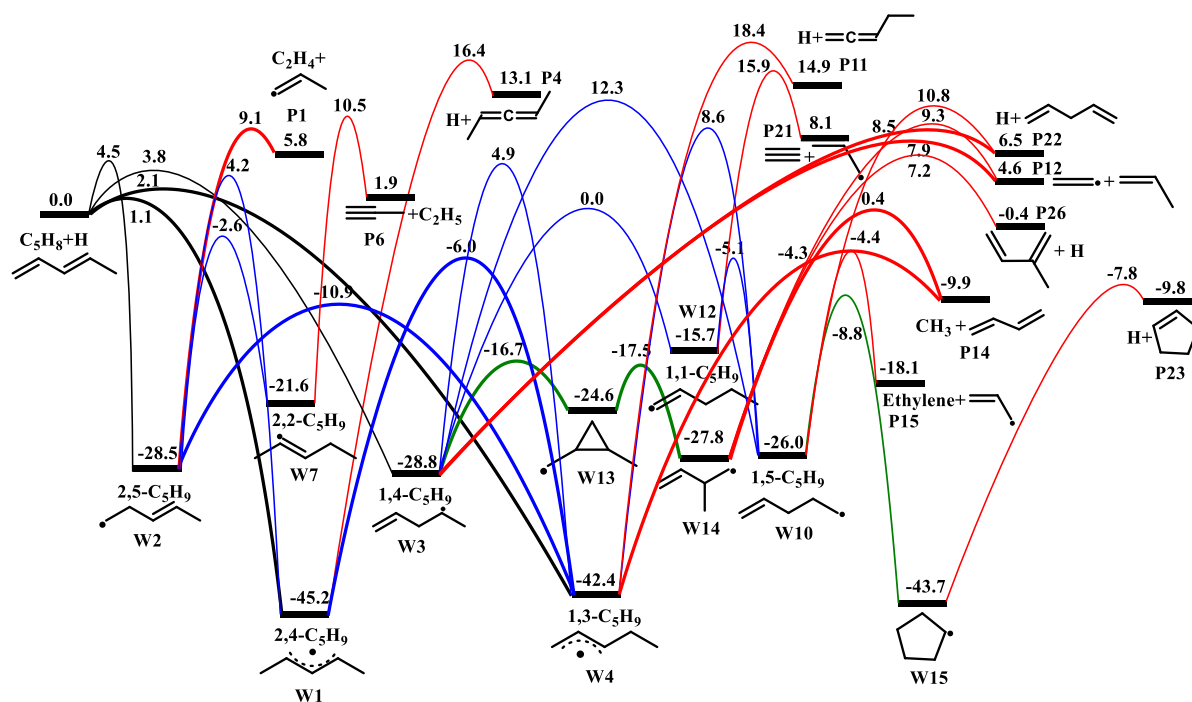


Figure 3. Simplified \dot{C}_5H_9 PES with ZPVE corrected restricted energies (in kcal mol^{-1}) relative to 1,3-pentadiene + \dot{H} .

Table 2. Zero-point vibrational energy corrected electronic energies (kcal mol⁻¹) relative to 1,3-pentadiene + Ḥ.

Label	Species	Energy		
		Spin-unrestricted	Spin-restricted	ΔE_{0K}
W1	2,4-Ċ ₅ H ₉	-44.5	-45.2	0.7
W2	2,5-Ċ ₅ H ₉	-28.4	-28.5	0.1
W3	1,4-Ċ ₅ H ₉	-28.7	-28.8	0.1
W4	1,3-Ċ ₅ H ₉	-41.8	-42.4	0.6
W7	2,2-Ċ ₅ H ₉	-21.3	-21.6	0.3
W10	1,5-Ċ ₅ H ₉	-26.0	-26.0	0.0
W13	1-methylene-cyclopropylmethyl	-24.5	-24.6	0.1
W14	3-methyl-1-buten-4-yl	-27.7	-27.8	0.1
W15	Cyclopentyl	-43.6	-43.7	0.1
R	1,3-pentadiene+Ḥ	0.0	---	---
P1	Ethylene + 1-propenyl	6.3	5.8	0.5
P6	Propyne + ethyl	1.9	1.9	0.0
P12	Vinyl + propene	5.1	4.6	0.5
P14	1,3-butadiene+methyl	-9.8	-9.9	0.1
P15	Ethylene + allyl	-17.5	-18.1	0.6
P22	1,4-pentadiene+Ḥ	6.5	---	---
P23	Cyclopentene+ Ḥ	-9.8	---	---
P26	Isoprene +Ḥ	-0.4	---	---

Label	Reactant	Product	Energy		
			Spin-unrestricted	Spin-restricted	ΔE_{0K}
TS1	R	W1	2.3	1.1	1.2
TS2	R	W2	5.8	4.5	1.3
TS3	R	W3	5.0	3.8	1.2
TS4	R	W4	3.4	2.1	1.3
TS10	W1	W2	4.8	4.2	0.6
TS11	W1	W4	-5.8	-6.0	0.2
TS16	W2	W4	-10.5	-10.9	0.4
TS18	W2	W7	-2.0	-2.6	0.6
TS21	W2	P1	10.0	9.1	0.9
TS22	W3	W4	5.5	4.9	0.6
TS23	W3	W10	12.5	12.3	0.2
TS26	W3	W13	-16.3	-16.7	0.4
TS28	W3	P12	8.8	7.9	0.9
TS29	W3	P22	8.8	8.5	0.3
TS33	W4	W10	9.2	8.6	0.6
TS37	W4	P14	-2.9	-4.3	1.4
TS49	W7	P6	11.7	10.5	1.2
TS61	W10	W15	-8.2	-8.8	0.6
TS63	W10	P15	-3.2	-4.4	0.8
TS64	W10	P22	11.2	10.8	0.4
TS71	W13	W14	-17.1	-17.5	0.4
TS76	W14	P12	10.2	9.3	0.9
TS77	W14	P14	1.6	0.4	1.2
TS78	W14	P26	8.1	7.2	0.9
TS79	W15	P23	-7.5	-7.8	0.3

- **Pressure dependency of important reaction channels**

At infinite pressures, thermal equilibration is maintained and the reacting mixture has a Boltzmann distribution.⁵⁷ However, at lower pressures, collisions are not sufficiently rapid to

maintain a Boltzmann distribution, and the competition between thermal equilibration via collisional energy transfer and the dissociation process results in the pressure-dependence of the reaction rates. The temperature- and pressure-dependent rate constants for reactions on the \dot{C}_5H_9 PES are calculated in the temperature range 300–2000 K at pressures of 0.01 to 100 atm, with the electronic structure energies for species on the simplified \dot{C}_5H_9 PES calculated at the higher, RO-aug-cc-VXZ (where $X = T$ and Q), level of theory. The modified-Arrhenius rate constant equation is used to fit the rate constants at 0.01, 0.1, 1, 10, 100 atm over the available temperature range, with the fitted Arrhenius parameters provided in Chemkin format as Supporting Information.

In the following Section, the pressure dependencies of important reactions on the \dot{C}_5H_9 PES are discussed and compared where literature data exist. The important reactions can be divided into two types, namely unimolecular and bimolecular reactions. The total rate constants and the product branching ratios are also discussed for important unimolecular reactions. For important bimolecular reactions, the high-pressure limiting, and the temperature- and pressure-dependent total rate constants, product branching ratios, and the competition between addition and abstraction reactions are discussed.

The rate constants for some reactions become undefined at high temperatures when their rates of chemical equilibration exceed the rates of collisional relaxation,⁵⁸ thus the pressure-dependent rate constants are not always available over the entire temperature range. Based on Miller and Klippenstein's work,⁵⁸ such phenomena occurs when species equilibrate with each other as rapidly as their internal energy relaxes and the two species become chemically indistinguishable.⁵⁹ So that we can discuss the branching ratios of important \dot{C}_5H_9 radicals and bimolecular reactants over a wide range of temperature and pressure for important reaction pathways which do not have definable rate constants at intermediate and high temperatures in following discussion, we have extrapolated their pressure-dependent rate constants by fitting Arrhenius parameters based on rate constant points at low and/or intermediate temperatures. Since the rate constants for these reactions become undefinable at lower temperatures as pressure decreases, the branching ratios are discussed only at $p > 1$ atm. The extrapolated rate constants and their resulting branching ratios are provided in the figure captions where extrapolations are applied.

○ **Bimolecular reactions**

1,3-C₅H₈ + H

The total pressure-dependent rate constants for 1,3-C₅H₈ + H → products are compared with the corresponding high-pressure limiting rate constants and are shown in Figure 4(a). The pressure fall-off in rate constants increase as temperature increases with the $k(T, p)/k_\infty$ ratio decreasing from 0.7 at 1000 K to 0.5 at 2000 K at a pressure of 0.01 atm. This finding is consistent with the general conclusion that deviations from the high-pressure limiting are particularly severe for small molecules at higher temperatures and lower pressures.⁵⁷ The fall off at 1200 K and 1 atm is about 56%, with similar conditions widely used for laminar flame and shock tube experiments. It is also noticeable that, even at 100 atm, the fall-off in rate constant is a factor of two at 2000 K. Hence, the $k_{\text{total}}(1,3\text{-C}_5\text{H}_8 + \dot{\text{H}} \rightarrow \text{products})$ have shown an obvious pressure-dependency and the pressure-dependent rate constants should be used for accurate model predictions, especially at low pressures and high temperatures.

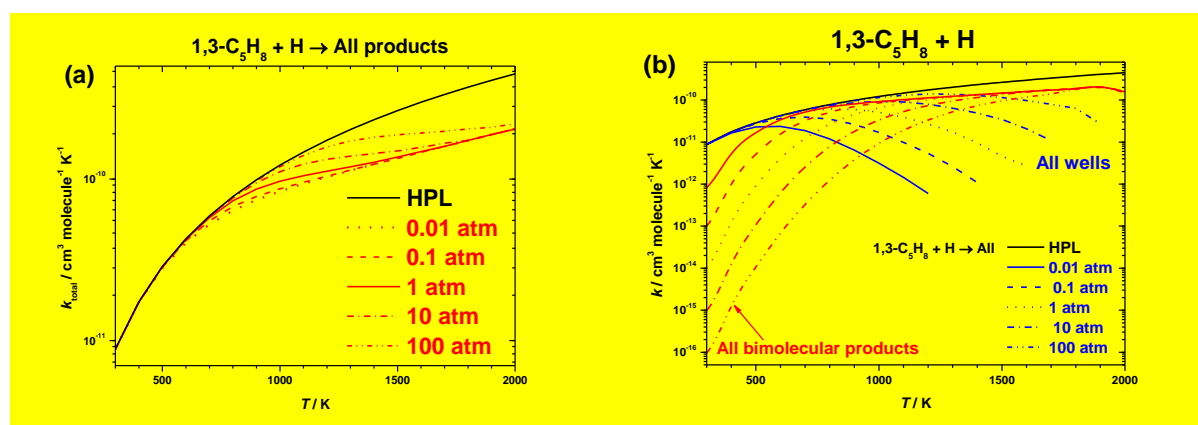


Figure 4. (a) The pressure-dependent rate constants and high-pressure limiting rate constants for 1,3-pentadiene + H → all products as a function of temperature. (b) The pressure-dependent and high-pressure limiting rate constants for 1,3-pentadiene + H → thermodynamically stabilized wells and bimolecular products at 0.01, 0.1, 1, 10, and 100 atm.

As the temperature and pressure dependence of a chemical rate constant arises from a complex interplay between chemical and collisional processes averaged over thermal distributions of reactant and collisional energies,⁵⁷ the pressure-dependent $k(1,3\text{-C}_5\text{H}_8 + \dot{\text{H}} \rightarrow \text{all bimolecular products})$ and $k(1,3\text{-C}_5\text{H}_8 + \dot{\text{H}} \rightarrow \text{all wells})$ are compared as a function of temperature and plotted in Figure 4(b). The $k(1,3\text{-C}_5\text{H}_8 + \dot{\text{H}} \rightarrow \text{all wells})$ are not available at high temperatures as their rates of chemical equilibration exceed the rates of collisional relaxation⁵⁸. The k_{Wells} is shown to have a positive pressure dependence with the collision

stabilization getting stronger as pressure increases. For a specific pressure, k_{Wells} decreases as temperature increases, while k_{Prods} shows the opposite trend, which indicates that the production of the thermodynamically stabilized wells are preferred at low temperatures and high pressures, and the production of the bimolecular products are preferred at high temperatures and low pressures.

The branching ratios (BRs) for important products generated from $\dot{\text{H}}$ addition to 1,3-pentadiene at 1 atm are plotted in Figure 5(a). The formation of 2,4- $\dot{\text{C}}_5\text{H}_9$ radicals is shown to be mostly favoured at low temperatures with a branching ratio of 86.6% at 300 K, with ~12.0% 1,3- $\dot{\text{C}}_5\text{H}_9$ radical also formed. Hence, the formation of allylic $\dot{\text{C}}_5\text{H}_9$ radicals is dominant at low temperatures. Allylic radical production is overtaken by the production of 1,3- $\text{C}_4\text{H}_6 + \dot{\text{C}}\text{H}_3$ radicals at 1000 K, which has the largest branching ratio of 76.9% at 1400 K, decreasing to 64.3% at 2000 K. At high temperatures, there are also other bimolecular products formed, and their branching ratios are 11.4% for $\text{C}_2\text{H}_4 + 1\text{-propenyl}$ radicals, 9.6% for $1,4\text{-C}_5\text{H}_8 + \dot{\text{H}}$ atoms, 8.9% for C_2H_3 radicals + C_3H_6 and 2.4% for $2,3\text{-C}_5\text{H}_8 + \dot{\text{H}}$ atoms at 2000 K.

To analyse the pressure dependence of product branching ratios, those for the formation of 2,4- $\dot{\text{C}}_5\text{H}_9$ radicals and the 1,3- $\text{C}_4\text{H}_6 + \dot{\text{C}}\text{H}_3$ radical pathway at 0.01, 0.1, 1, 10 and 100 atm are compared and plotted in Figure 5(b). The branching ratios of these two important channels show significant temperature and pressure dependencies. The branching ratios at different pressures show similar trends with various cross-over points for BR(2,4- $\dot{\text{C}}_5\text{H}_9$) and BR(1,3- $\text{C}_4\text{H}_6 + \dot{\text{C}}\text{H}_3$). At 1000 K, the BR(2,4- $\dot{\text{C}}_5\text{H}_9$) increases from 2.6% to 62.9% as the pressure increases from 0.01 to 100 atm, while the BR(1,3- $\text{C}_4\text{H}_6 + \dot{\text{C}}\text{H}_3$) decreases from 91.2% at 0.01 atm to 2.9% at 100 atm. Notably, the temperatures of the cross-over points vary from 580 K at 0.01 atm to 1560 K at 100 atm, while their corresponding branching ratios show small differences, they being $32.3\% < \text{BR}(2,4\text{-}\dot{\text{C}}_5\text{H}_9) \approx \text{BR}(1,3\text{-C}_4\text{H}_6 + \dot{\text{C}}\text{H}_3) < 39.8\%$. In general, the temperature and pressure dependencies of the rate constants should be considered when discussing important products and/or exploring their branching ratios.

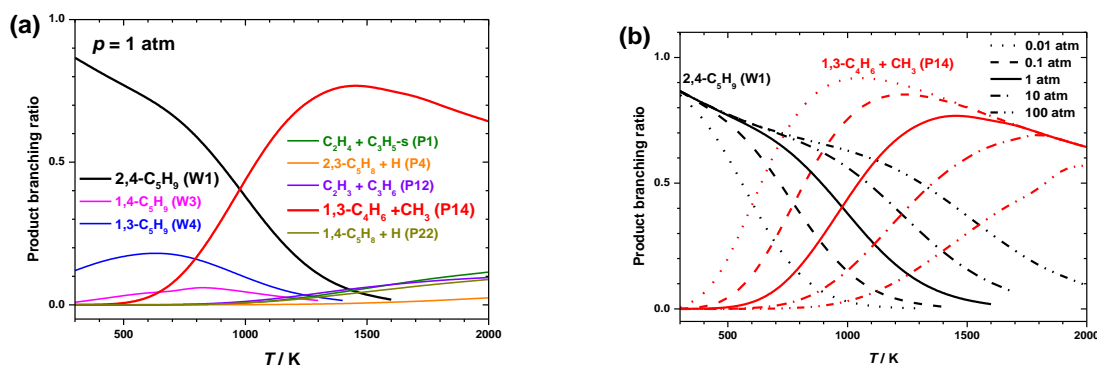


Figure 5. (a) The branching ratios for important products from $\dot{\text{H}}$ addition to 1,3-pentadiene at 1 atm, (b) The branching ratios for 2,4- $\dot{\text{C}}_5\text{H}_9$ radical (W1) and 1,3-butadiene + $\dot{\text{C}}\text{H}_3$ (P14) produced from $\dot{\text{H}}$ addition to 1,3-pentadiene at 0.01, 0.1, 1, 10, and 100 atm.

The PES and high-pressure limiting rate constants for H-atom abstraction reactions from 1,3-pentadiene by $\dot{\text{H}}$ atoms was illustrated in Part I, and the total rate constants for H-atom abstraction reactions are compared with the pressure-dependent total rate constants for $\dot{\text{H}}$ atom addition reactions of 1,3-pentadiene herein. Figure 6 shows that H-atom abstraction reactions are negligible at low temperatures compared with $\dot{\text{H}}$ atom addition reactions. However, the increased importance of H-atom abstraction reactions is observed at higher temperatures, with the $k_{0.01\text{atm}}(\text{addition})/k_{\text{total}}(\text{abstraction})$ ratios being within an order of magnitude at temperatures above 1200 K and are close to a factor of two at 2000 K.

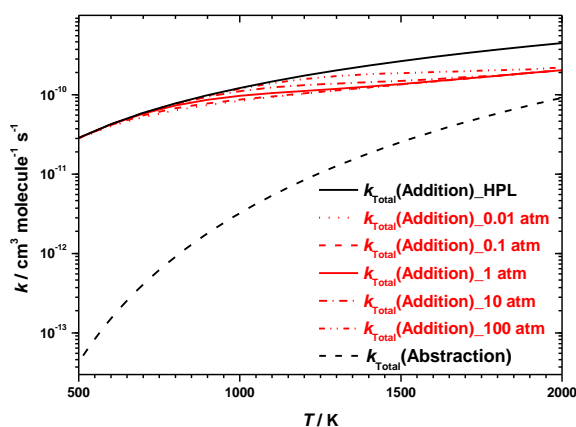


Figure 6. The total rate constant comparisons between the H-atom abstraction reactions by $\dot{\text{H}}$ atoms and $\dot{\text{H}}$ atom addition reactions from/to 1,3-pentadiene.

1,4- $\text{C}_5\text{H}_8 + \dot{\text{H}}$

The branching ratios for important products generated from $\dot{\text{H}}$ atom addition to 1,4-pentadiene at 1 atm are plotted in Figure 7(a). At 1 atm and low temperatures (< 900 K), the

production of 1,4- \dot{C}_5H_9 radicals dominates, followed by 3-methyl-1,4-butadienyl radical (3Me-1,4- C_4H_6). The formation of 1,3- $C_4H_6 + \dot{C}H_3$ radicals dominates in the temperature range 1000–1600 K, but is then overtaken by the production of \dot{C}_2H_3 radical + C_3H_6 at ~1600 K and $C_2H_4 + \dot{C}_3H_5$ -a at ~1700 K. It can be seen that the dominance of the formation of 1,3-butadiene, which is a lower hierarchy diene compared to 1,3- and 1,4-pentadiene, is weaker for \dot{H} addition to 1,4-pentadiene and the formation of $C_2 + C_3$ ($\dot{C}_2H_3 + C_3H_6$, $C_2H_4 + \dot{C}_3H_5$ -a) bimolecular products are more favoured at high temperatures.

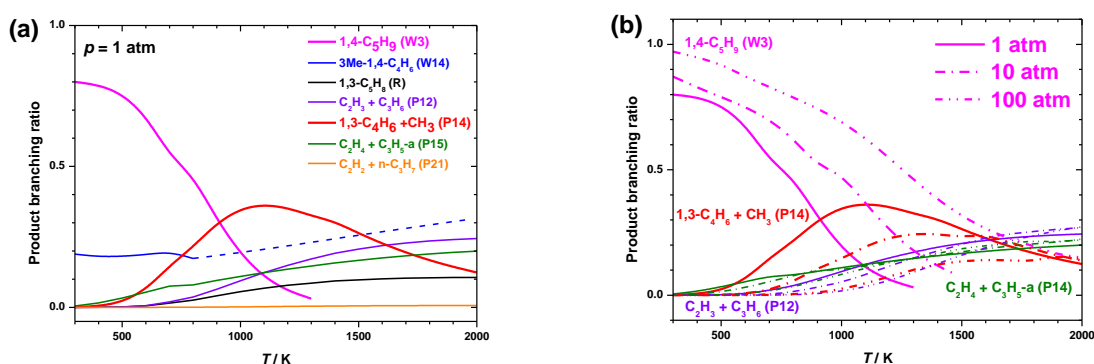


Figure 7. (a) The branching ratios for important products generated by \dot{H} atom addition to 1,4-pentadiene at 1 atm, with $k(1,4-C_5H_8 + H \rightarrow 3Me-1,4-C_4H_6)$ extrapolated from 800 K to 2000 K. (b) The branching ratios for 1,4- \dot{C}_5H_9 radical (W3), 1,3-butadiene + $\dot{C}H_3$ (P14), $\dot{C}_2H_3 + C_3H_6$ (P12), and $C_2H_4 + \dot{C}_3H_5$ -a (P15) produced from \dot{H} atom addition to 1,4-pentadiene at 1, 10, and 100 atm. The BRs are calculated with extrapolated $k(1,4-C_5H_8 + H \rightarrow 3Me-1,4-C_4H_6)$ including in total rate constants.

Due to the absence of $k(1,4-C_5H_8 + H \rightarrow 3Me-1,4-C_4H_6)$ at temperatures above 700 K, the branching ratios of the other products, which are relied on total rate constants, can't be accurately predicted. Hence, $k(1,4-C_5H_8 + H \rightarrow 3Me-1,4-C_4H_6)$ are extrapolated from 800 K to 2000 K and included in total rate constant calculations. The branching ratios at 1, 10 and 100 atm for the formation of 1,4- \dot{C}_5H_9 radical and three major bimolecular products (1,3- $C_4H_6 + \dot{C}H_3$, $\dot{C}_2H_3 + C_3H_6$, $C_2H_4 + \dot{C}_3H_5$ -a) are compared. As shown in Figure 7(b), the production of 1,4- \dot{C}_5H_9 radicals has a strong positive pressure-dependence and negative temperature-dependence. The branching ratios of 1,3- $C_4H_6 + \dot{C}H_3$ increases with temperature in the first place, then decreases to about 14% at 2000 K due to the competition of the other bimolecular products. The formation of these three bimolecular products all show negative pressure-dependencies and their branching ratios tend to converge at high temperatures. At

2000 K and different pressures, the most important product for $\dot{\text{H}}$ atom addition to 1,4-pentadiene is $\dot{\text{C}}_2\text{H}_3 + \text{C}_3\text{H}_6$, followed by $\text{C}_2\text{H}_4 + \dot{\text{C}}_3\text{H}_5\text{-a}$, $1,3\text{-C}_4\text{H}_6 + \dot{\text{C}}\text{H}_3$, and $1,3\text{-C}_5\text{H}_8 + \dot{\text{H}}$.

The PES for H-atom abstraction reactions of 1,4-pentadiene by $\dot{\text{H}}$ atoms is described in detail in Figure S2. The high-pressure limiting rate constants for H-atom abstraction reactions of 1,4-pentadiene by $\dot{\text{H}}$ atoms are shown in Figure 8(a) and compared with those for H-atom abstraction reactions from 1,3-butadiene⁴³ and 1,3-pentadiene. It can be clearly seen that abstraction of an allylic hydrogen atom from 1,4-pentadiene and/or 1,3-pentadiene to form a doubly allylic 1,4-pentadien-3-yl (or 1,3-pentadien-5-yl) radical is favoured over the abstraction of vinylic hydrogen atoms. It is noticeable that the barrier height for H-atom abstraction from the allylic site on 1,4-pentadiene is $2.8 \text{ kcal mol}^{-1}$ lower than that for H-atom abstraction from the allylic site on 1,3-pentadiene. As a result, rate constants for abstraction from 1,4-pentadiene are about an order of magnitude faster than from 1,3-pentadiene at 300 K and become similar to those for H-atom abstraction from the allylic site on 1,3-pentadiene at 2000 K. At temperatures below 700 K, the rate constants for H-atom abstraction from the secondary vinylic sites are faster than those from the primary vinylic sites, thereafter there is no appreciable difference between these two reaction classes at higher temperatures. For H-atom abstraction from the secondary vinylic and primary vinylic sites by $\dot{\text{H}}$ atoms, the trend for rate constants is $k_\infty(1,3\text{-pentadiene}) < k_\infty(1,3\text{-butadiene}) < k_\infty(1,4\text{-pentadiene})$; and for H-atom abstraction from the allylic sites, the trend for rate constants is $k_\infty(1,3\text{-pentadiene}) < k_\infty(1,4\text{-pentadiene})$.

The total rate constants for H-atom abstraction reactions of 1,4-pentadiene are compared with the $\dot{\text{H}}$ -addition pressure-dependent total rate constants in Figure 8(b). Similar to H-atom abstraction reactions from 1,3-pentadiene, H-atom abstraction from 1,4-pentadiene is negligible at low temperatures with the $k_{0.01\text{atm}}(\text{addition})/k_{\text{total}}(\text{abstraction})$ ratio decreasing to within an order of magnitude at temperatures above 1000 K and 2.5 times at 2000 K. What stands out is that $k_{\text{total}}(\text{addition})$ of $1,4\text{-C}_5\text{H}_8 + \dot{\text{H}}$ shows a weaker pressure-dependence with the fall-off of the rate constants compared with the high-pressure limiting rate constants being within 26%. Considering the strong pressure-dependence of the product branching ratios, pressure-dependent rate constants for $1,4\text{-C}_5\text{H}_8 + \dot{\text{H}}$ should still be used to accurately predict product yields.

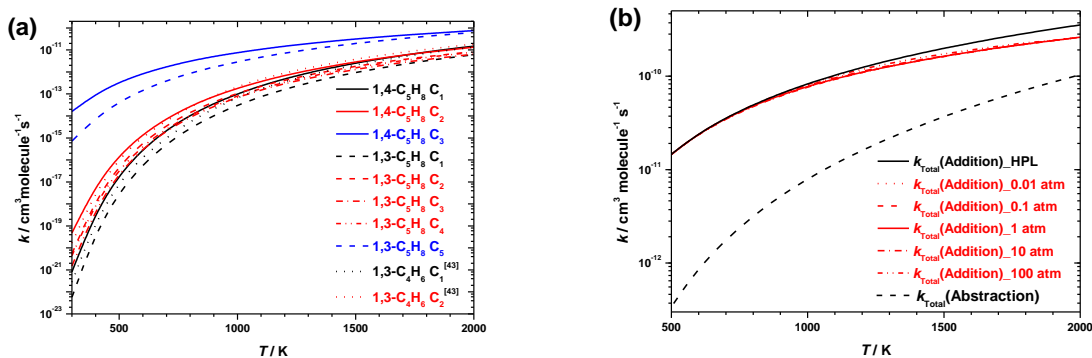


Figure 8. (a) Rate constant comparisons for H-atom abstraction reactions of 1,4-pentadiene by $\dot{\text{H}}$ atoms. The solid lines represent H-atom abstraction reactions from 1,4-pentadiene, while the dash and dot lines represent H-atom abstraction reactions from 1,3-pentadiene and 1,3-butadiene⁴³ by $\dot{\text{H}}$ atoms, respectively. The black lines represent H-atom abstraction from the primary vinylic sites of these three dienes, the red lines represent H-atom abstraction from the secondary vinylic sites, and the blue lines represent H-atom abstraction from the allylic sites. (b) The total rate constant comparisons between the H-atom abstraction reactions by $\dot{\text{H}}$ atoms and $\dot{\text{H}}$ -addition reactions from/to 1,4-pentadiene.

Cyclopentene + $\dot{\text{H}}$

The branching ratios for important products at 1 atm generated from $\dot{\text{H}}$ atom addition to cyclopentene (cyC_5H_8) are plotted in Figure 9(a). The direct formation of cyclopentyl radical ($\text{cy}\dot{\text{C}}_5\text{H}_9$) via $\dot{\text{H}}$ atom addition to cyclopentene dominates at low temperatures (< 1100 K) and is then overtaken by the formation of $\text{C}_2\text{H}_4 + \dot{\text{C}}_3\text{H}_5\text{-a}$ with a largest branching ratio of 96.0%. A small amount of 1,5- $\dot{\text{C}}_5\text{H}_9$ radical ($\sim 4\%$) is formed at low temperatures and less than 3% of the flux proceeds through $1,4\text{-C}_5\text{H}_8 + \dot{\text{H}}$ at high temperatures. The branching ratios of $\text{cy}\dot{\text{C}}_5\text{H}_9$ radical and $\text{C}_2\text{H}_4 + \dot{\text{C}}_3\text{H}_5\text{-a}$ radical at different pressures are shown in Figure 9(b) with $\text{BR}(\text{cy}\dot{\text{C}}_5\text{H}_9)$ increasing as pressure increases and $\text{BR}(\text{C}_2\text{H}_4 + \dot{\text{C}}_3\text{H}_5\text{-a})$ showing the opposite trend. Although $\text{BR}(\text{C}_2\text{H}_4 + \dot{\text{C}}_3\text{H}_5\text{-a})$ at different pressures converge at high temperatures, the pressure-dependent rate constants for $\text{cyC}_5\text{H}_8 + \dot{\text{H}}$ still need to be considered at temperatures below 1900 K in order to simulate the product branching ratios.

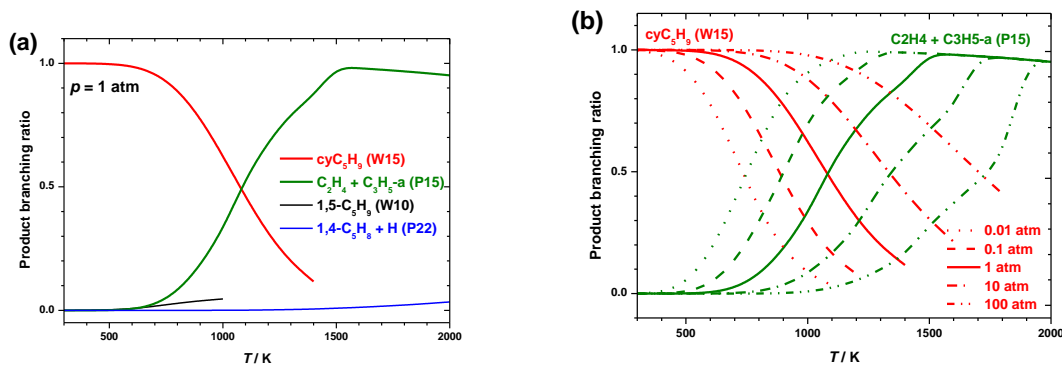


Figure 9. (a) The branching ratios for important products from $\dot{\text{H}}$ atom addition to cyC_5H_8 at 1 atm, (b) the branching ratios for $\text{cy}\dot{\text{C}}_5\text{H}_9$ radical (W15) and $\text{C}_2\text{H}_4 + \dot{\text{C}}_3\text{H}_5\text{-a}$ (P15) produced from $\dot{\text{H}}$ atom addition to cyC_5H_8 at 0.01, 0.1, 1, 10, and 100 atm.

The PES for H-atom abstraction reactions of cyC_5H_8 by $\dot{\text{H}}$ atoms are described in detail in Figure S3. The formation of 1,3- and 1,4-cyclopentenyl radicals via H-atom abstraction from cyclopentene has been included in Al Rashidi's cyclopentane mechanism, of which the rate constants for the former reaction are obtained by analogy to H-atom abstraction reaction from 1-hexene, while the rate constants for the formation of 1,4-cyclopentenyl radical is estimated by applying a rate rule for secondary allylic H-atom abstraction from alkenes⁶⁰. Figure 10(a) shows that the $k(1,3\text{-cyclopentenyl})$ estimated by Al Rashidi agrees with this work with differences within a factor of two at temperatures above 600 K. Meanwhile, the $k(1,4\text{-cyclopentenyl})$ obtained by analogy to H-atom abstraction from 1-hexene is 2–3 times slower than that calculated here. The comparisons indicate that H-atom abstraction from cyclopentene can be estimated using a rate rule by analogy for abstraction from alkenes with uncertainties within a factor of three.

The total rate constants for $\text{cyC}_5\text{H}_8 + \dot{\text{H}}$ via addition and abstraction reactions are compared in Figure 10(b). The fall-off of $k_{\text{total}}(\text{addition})$ at different pressures compared to the high-pressure limiting rate constants can reach up to a factor of 2.4 at 2000 K. In contrast to the total rate constant comparisons for 1,3- and 1,4- $\text{C}_5\text{H}_8 + \dot{\text{H}}$, H-atom abstraction of cyclopentene is competitive with $\dot{\text{H}}$ atom addition, even at low temperatures, with the deviation between $k_{\text{total}}(\text{addition})$ and $k_{\text{total}}(\text{abstraction})$ within an order of magnitude at 500 K. In addition, $k_{\text{total}}(\text{abstraction})$ overtakes $k_{\text{total}}(\text{addition})$ at 0.01 atm and ~ 1100 K and $k_{\infty}(\text{addition})$ at 1800 K. Hence, H-atom abstraction reactions are relatively more important for cyclopentene than for 1,3- and 1,4-pentadiene at the temperatures studied. Based on the branching ratio study presented in Figure 9, the product formed at temperatures below 400 K

is mainly $\text{cy}\dot{\text{C}}_5\text{H}_9$ radical. Hence, the $k(\text{cyC}_5\text{H}_8 + \dot{\text{H}} \rightarrow \text{cy}\dot{\text{C}}_5\text{H}_9)$ from Clarke's work, which is measured in a flow tube over temperature range 298–370 K and 50 Torr, is compared with our calculated results and shows good agreement with values being within 50% of one another.

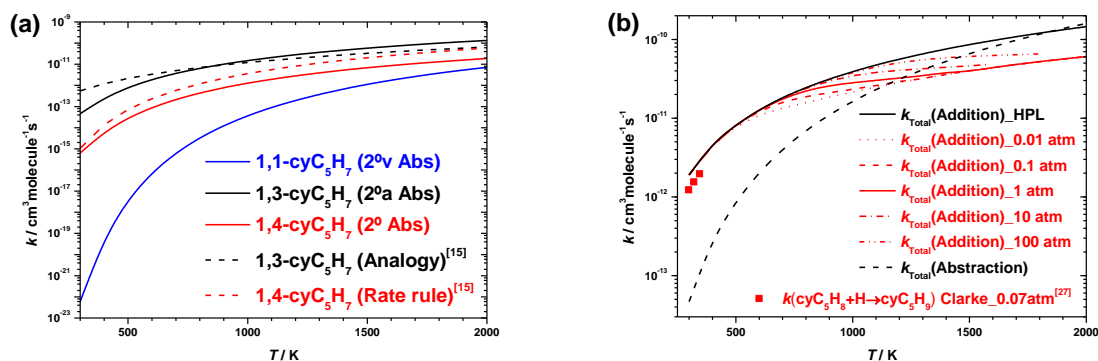


Figure 10. (a) Rate constant comparisons for H-atom abstraction reactions of cyC_5H_8 by $\dot{\text{H}}$ atoms from this work and literature.¹⁵ (b) The total rate constant comparisons between the H-atom abstraction reactions by $\dot{\text{H}}$ atoms and $\dot{\text{H}}$ -addition reactions from/to cyC_5H_8 . The red symbol represents experimental results by Clarke et al.²⁷ at 0.07 atm for $\text{cyC}_5\text{H}_8 + \dot{\text{H}} \rightarrow \text{cy}\dot{\text{C}}_5\text{H}_9$.

Ethylene + allyl

The branching ratios for important products at 1 atm generated by allyl radical addition to ethylene are plotted in Figure 11(a), with $k(\text{C}_2\text{H}_4 + \dot{\text{C}}_3\text{H}_5\text{-a} \rightarrow 1,5\text{-}\dot{\text{C}}_5\text{H}_9)$ extrapolated from 1400 K to 2000 K. The dominant product at 1 atm is $1,5\text{-}\dot{\text{C}}_5\text{H}_9$ radical at temperatures below 1700 K and $1,4\text{-C}_5\text{H}_8 + \dot{\text{H}}$ at higher temperatures. There are also small amounts of $\text{cy}\dot{\text{C}}_5\text{H}_9$ radicals (W15) and $\text{cyC}_5\text{H}_8 + \dot{\text{H}}$ atoms (P23) formed, with a maximum $\text{BR}(\text{cy}\dot{\text{C}}_5\text{H}_9)$ of 6.8% at 900 K and $\text{BR}(\text{cyC}_5\text{H}_8 + \dot{\text{H}})$ of 11.8% at 1500 K. The pressure-dependence of dominant product branching ratios for allyl radical addition to ethylene are shown in Figure 11(b). The branching ratios of important products show strong temperature- and pressure-dependencies. The $\text{BR}(1,5\text{-}\dot{\text{C}}_5\text{H}_9)$ increases rapidly as pressure increases from 1 atm to 100 atm at a specific temperature. While the $\text{BR}(1,4\text{-C}_5\text{H}_8 + \dot{\text{H}})$ has an opposite performance with larger decreases being found as the pressure increases from 1–100 atm at temperatures above 1500 K. Due to the dominant product branching ratios for $\text{C}_2\text{H}_4 + \dot{\text{C}}_3\text{H}_5\text{-a}$ are very sensitive to pressure, the pressure-dependent rate constants should be used for simulations related to this system.

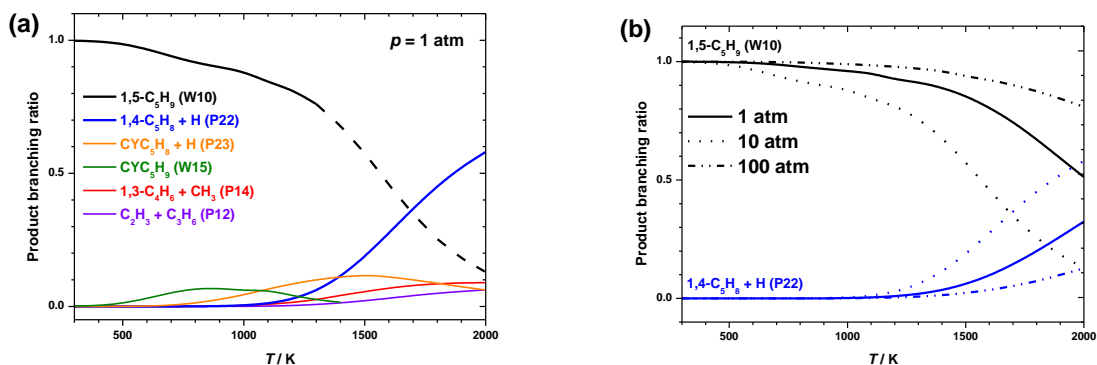


Figure 11. (a) The branching ratios for important products from allyl addition to ethylene at 1 atm, with $k(\text{C}_2\text{H}_4 + \dot{\text{C}}_3\text{H}_5\text{-a} \rightarrow 1,5\text{-}\dot{\text{C}}_5\text{H}_9)$ extrapolated from 1400 K to 2000 K. (b) the branching ratios for 1,5- $\dot{\text{C}}_5\text{H}_9$ (W10), cy $\dot{\text{C}}_5\text{H}_9$ (W15), 1,4- $\text{C}_5\text{H}_8 + \dot{\text{H}}$ (P22) and cy $\text{C}_5\text{H}_8 + \dot{\text{H}}$ (P23) produced from allyl addition to ethylene at 0.01, 1.0 and 100 atm. The BRs are calculated with $k(\text{C}_2\text{H}_4 + \dot{\text{C}}_3\text{H}_5\text{-a} \rightarrow 1,5\text{-}\dot{\text{C}}_5\text{H}_9)$, which are including in total rate constants, extrapolated over a temperature range of 1400–2000 K at 1 atm, 1600–2000 K at 10 atm, and 1900–2000 K at 100 atm.

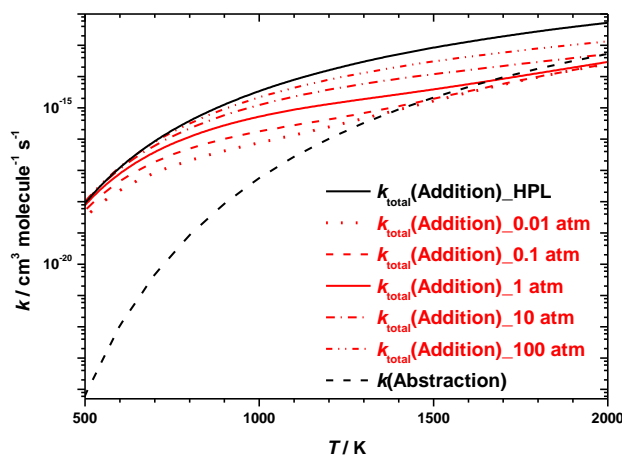


Figure 12. The total rate constant comparisons between the H-atom abstraction reactions and addition reactions of allyl radical with ethylene. The total rate constants for addition reactions include $k(\text{C}_2\text{H}_4 + \dot{\text{C}}_3\text{H}_5\text{-a} \rightarrow 1,5\text{-}\dot{\text{C}}_5\text{H}_9)$ extrapolated over a temperature range of 1100–2000 K at 0.01 atm, 1200–2000 K at 0.1 atm, 1400–2000 K at 1 atm, 1600–2000 K at 10 atm, and 1900–2000 K at 100 atm.

The rate constants for the H-atom abstraction reaction by allyl radicals from ethylene (reverse reaction of H-atom abstraction reaction of propene by vinyl radicals) are compared

to its addition reactions at different pressures and high-pressure limiting in Figure 12. The pressure-dependent total rate constants have a fall-off in the intermediate temperature range, mainly due to the decrease of $k(\text{C}_2\text{H}_4 + \text{C}_3\text{H}_5\text{-a} \rightarrow 1,5\text{-C}_5\text{H}_9)$. As shown in the comparison, $k(\text{Abstraction})$ overtake the $k_{\text{total}}(0.01 \text{ atm})$ at 1500 K and are close to $k_{\text{total}}(10 \text{ atm})$ at 2000 K. Hence, the abstraction reaction of $\text{C}_2\text{H}_4 + \text{C}_3\text{H}_5\text{-a}$ is important at high temperatures and needs to be included in the mechanism development.

Vinyl + propene

The branching ratios for important products generated from vinyl radical addition to propene at different pressures are plotted in Figure 13(a) and (b), respectively. At 1.0 atm, the production of 1,4- $\dot{\text{C}}_5\text{H}_9$ radical (W3) is dominant at temperatures below 900 K, and 3-methyl-1-buten-4-yl radical (W14) also plays an important role with BRs close to 20% over the temperature range of 300–2000 K. At temperatures above 1200 K, the important products are 1,3- $\text{C}_4\text{H}_6 + \dot{\text{C}}\text{H}_3$ followed by 1,4- $\text{C}_5\text{H}_8 + \dot{\text{H}}$ and 1,3- $\text{C}_5\text{H}_8 + \dot{\text{H}}$ with BRs of 33.3%, 27.7% and 13.0% at 2000 K, respectively.

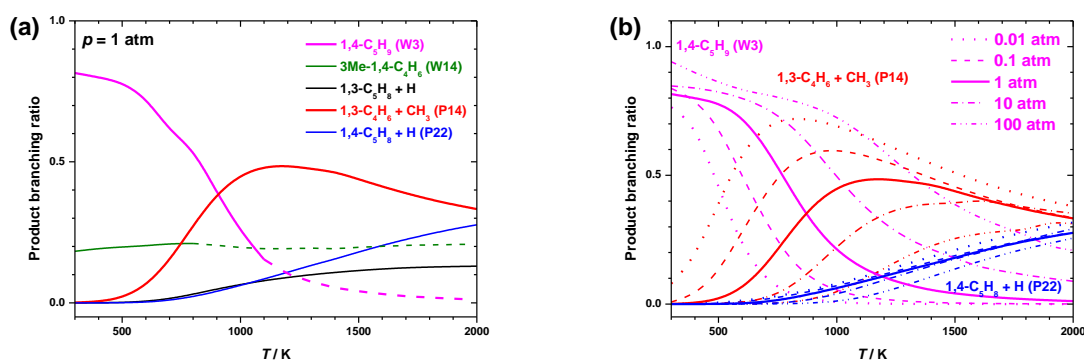


Figure 13. (a) The branching ratios for important products from vinyl addition to propene at 1 atm, with $k(\dot{\text{C}}_2\text{H}_3 + \text{C}_3\text{H}_6 \rightarrow 1,4\text{-}\dot{\text{C}}_5\text{H}_9)$ extrapolated from 1200 K to 2000 K and $k(\dot{\text{C}}_2\text{H}_3 + \text{C}_3\text{H}_6 \rightarrow 3\text{Me-1,4-}\dot{\text{C}}_4\text{H}_6)$ extrapolated from 800 K to 2000 K. (b) The branching ratios for 1,4- $\dot{\text{C}}_5\text{H}_9$ (W3), 3-methyl-1-buten-4-yl (W14), 1,3- $\text{C}_5\text{H}_8 + \dot{\text{H}}$, 1,3- $\text{C}_4\text{H}_6 + \dot{\text{C}}\text{H}_3$ (P14) and 1,4- $\text{C}_5\text{H}_8 + \dot{\text{H}}$ (P22) produced from vinyl addition to propene at 0.01, 0.1, 1, 10 and 100 atm. The total rate constants are calculated with extrapolated $k(\dot{\text{C}}_2\text{H}_3 + \text{C}_3\text{H}_6 \rightarrow 1,4\text{-}\dot{\text{C}}_5\text{H}_9)$ and $k(\dot{\text{C}}_2\text{H}_3 + \text{C}_3\text{H}_6 \rightarrow 3\text{Me-1,4-}\dot{\text{C}}_4\text{H}_6)$, where no available rate constants exist.

As shown in Figure 13(b), at 0.01 atm and temperatures above 500 K, the production of 1,3- $\text{C}_4\text{H}_6 + \dot{\text{C}}\text{H}_3$ is the most favoured and its cross-over point with BR(1,4- $\dot{\text{C}}_5\text{H}_9$) changes from 500 K to 1700 K as the pressure increases from 0.01 atm to 100 atm. The production of

1,4-C₃H₈ + $\dot{\text{H}}$ is also important at high temperatures which doesn't show a strong pressure-dependence. Hence, the dominant product branching ratios of vinyl radical addition to propene show strong temperature- and pressure-dependencies, and $k(T, p)$ need to be used to quantitatively predict product formation.

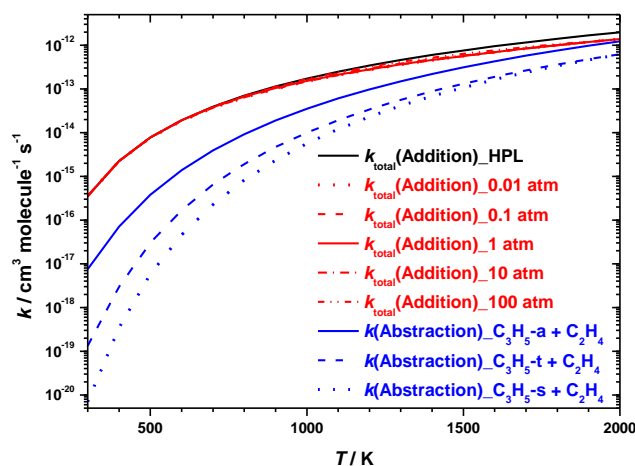


Figure 14. The total rate constant comparisons between the H-atom abstraction reactions and addition reactions of vinyl radical and propene.

The rate constants for H-atom abstraction reaction of propene by vinyl radicals are compared with its addition reactions at different pressures and high-pressure limiting rate constants in Figure 14. The total addition rate constants are shown to have weak pressure dependence with a largest fall-off of 43% at 2000 K at pressures in the range 0.01–100 atm. The PES for H-atom abstraction reactions of C₃H₆ by $\dot{\text{C}}_2\text{H}_3$ radicals are described in detail in Figure S4. Vinyl radicals can abstract the allylic hydrogen atom from propene forming allyl radicals and ethylene, followed by forming 1-propen-2-yl radical and ethylene via abstraction of the secondary vinylic hydrogen atom on the central carbon, and finally abstraction of the two primary vinylic hydrogen atoms on the terminal carbon. As one might anticipate, the barrier heights for these three channels are 6.2, 10.0 and 12.1 kcal mol⁻¹, respectively. The terminal abstractions can form cis- and trans-1-propen-1-yl radicals which have very similar barriers and the averaged rate constants are plotted in Figure 14. The abstraction reactions for $\dot{\text{C}}_2\text{H}_3 + \text{C}_3\text{H}_6$ are non-negligible at high temperatures with the difference between $k(\dot{\text{C}}_2\text{H}_3 + \text{C}_3\text{H}_6 \rightarrow \text{C}_2\text{H}_4 + \dot{\text{C}}_3\text{H}_5\text{-a})$ and $k_{\text{total}}^{\text{HPL}}(\dot{\text{C}}_2\text{H}_3 + \text{C}_3\text{H}_6 \rightarrow \text{All products})$ being within a factor of two at temperatures above 1700 K. For the pressure-dependent rate constants for addition reactions, the difference decreases to within a factor of two at temperatures above 1400 K.

Therefore, H-atom abstraction reaction from propene by vinyl radicals are important and need to be considered at high temperatures.

Goldsmith et al.^{11, 61-62} carried out flow reactor experiments on vinyl + alkenes in the temperature range 300–700 K and at pressures of 15–100 Torr, where the alkenes include ethylene, propene and butene isomers. They also studied vinyl + propene and its subsequent reactions at the G3 level of theory.¹¹ Li et al.⁴³ studied 1,3-butadiene + $\dot{\text{H}}$ and related reactions on the $\dot{\text{C}}_4\text{H}_7$ PES at the CCSD(T)/CBS//M06-2X/6-311++G(d,p) level of theory which includes vinyl addition to ethylene. The experimental and calculated rate constants for vinyl addition to different alkenes (ethylene, propene and butene isomers) at 0.13 atm are shown in Figure 15. For the experiments at 0.13 atm, the fastest reaction is vinyl radical addition to propene, followed by isobutene, 1-butene, ethylene, and 2-butene.⁶¹ The theoretical calculations also show that the rate constants for vinyl + propene are faster than vinyl + ethylene, and the averaged rate constant ratio ($k_{\text{propene} + \text{vinyl}} / k_{\text{ethylene} + \text{vinyl}}$) for experiments and theoretical calculations is 1.8 and 1.7, respectively. Thus, the trends in our theoretical calculations for vinyl + propene and vinyl + ethylene are consistent with the experimental results.

In comparison with the experimental data at 0.13 atm, the rate constants for vinyl radical addition to propene producing all products calculated in this work are about two to three times slower in the temperature range 300–700 K. Goldsmith et al.^{11, 61-62} also carried out theoretical calculations for $\text{C}_3\text{H}_6 + \dot{\text{C}}_2\text{H}_3$ which were in very good agreement with their experiments in the temperature range 350–700 K. Since we are using different levels of theory for theoretical calculations, detailed studies need to be carried out to analyse the possible reasons for the differences between the two theoretical studies. As shown in Figure 13, 1,3-butadiene + $\dot{\text{C}}\text{H}_3$ and 1,4- $\dot{\text{C}}_5\text{H}_9$ radicals are the dominant products for vinyl radical addition to propene at the experimental conditions. Furthermore, the k_∞ for vinyl + propene \rightarrow 1,4- $\dot{\text{C}}_5\text{H}_9$ (R1) are over an order of magnitude faster than those for vinyl + propene \rightarrow 3-methyl-1-buten-4-yl and/or vinyl + propene \rightarrow ethylene + allyl at temperature range 300–700 K. Hence, R1 is selected as a representative reaction to analyse the influence of different levels of theory on rate constant calculations.

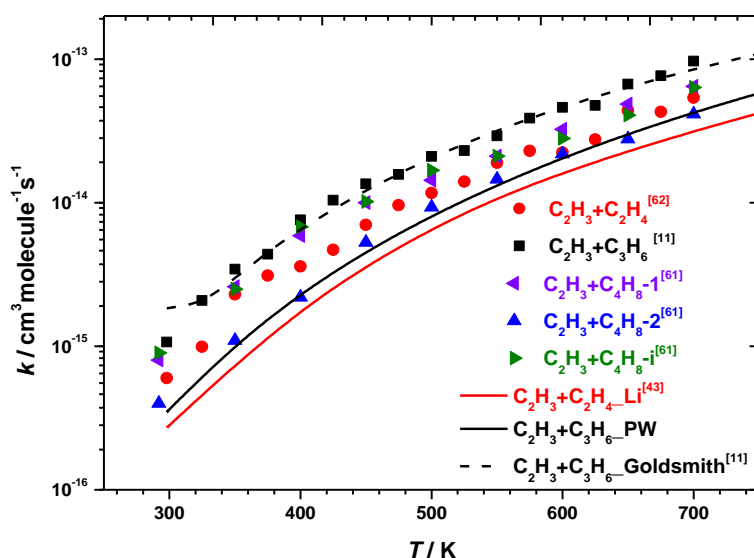


Figure 15. Comparison of the experimental and calculated rate constants for vinyl + alkenes (ethylene, propene and butene isomers) at 0.13 atm. Different symbols represent experimental results for different reactants: ● vinyl + ethylene,⁶² ■ vinyl + propene,¹¹ ◄ vinyl + 1-butene,⁶¹ ▲ vinyl + 2-butene,⁶¹ ► vinyl + isobutene.⁶¹ The red solid line represent calculated results from Li et al.⁴³ for vinyl + ethylene and the black dash line represent calculated results from Goldsmith et al.¹¹ for vinyl + propene.

The k_{∞} for R1 are recalculated using Thermo and Densum code of Multiwell⁶³⁻⁶⁵ at the level of theories used in this work and Goldsmith's study. The k_{∞} of Goldsmith's calculations are 3.8 times larger at 300 K than this work and the difference decreases to 2.5 times at 700 K. The partition function contains all of the thermodynamics information associated with the system, including internal energy, entropy, heat capacity, etc.⁶⁶ The partition function ratios for the TS of R1 taken from Goldsmith's work and this work are listed in Table 3. The comparison shows that: (i) at room temperature, the difference in energy barrier (0.2 kcal mol⁻¹ in R1) has the largest influence on the total ratio followed by the hindered-rotor treatment; (ii) the influence of vibrational partition functions (Q_{vib}) increases as temperature increases, these becoming dominant at temperatures above 700 K; (iii) the rotational partition functions (Q_{rot}) show smaller difference compared with other partition functions. These four partition function ratios are multiplied together to generate a total ratio to compare with the high-pressure limiting rate constant ratios of R1. The difference between these two ratios is within 20%, therefore, we can infer the difference between this work and Goldsmith's calculation is from the different theoretical methods used for: (i) geometry optimization and

vibrational frequency calculations, leading to differences in the prediction of vibrational partition functions Q_{vib} and rotational partition functions Q_{rot} ; (ii) single point energy calculation leading to 1.9 times difference at room temperature; (iii) hindered-rotor treatment which contribute to the 1.4 times difference of hindered-rotor partition function Q_{hindro} .

Table 3. Comparison of the partition function ratios between this work and literature for vinyl + propene \rightarrow 1,4- $\dot{\text{C}}_5\text{H}_9$.

T	$R(Q_{\text{vib}})$	$R(Q_{\text{rot}})$	$R(Q_{\text{hindro}})$	$R(\text{Barrier})$	$R(Q_{\text{Total}})$	$R(k_{\infty})$
300	1.17	1.07	1.40	1.86	3.26	3.84
400	1.23	1.07	1.29	1.59	2.70	3.22
500	1.28	1.07	1.22	1.44	2.41	2.88
600	1.32	1.07	1.18	1.35	2.25	2.66
700	1.35	1.07	1.15	1.29	2.14	2.52

In this work, SPE calculations are carried out using ROCCSD(T) with augmented cc-pVTZ basis set extrapolated to cc-pVQZ and the uncertainty for CCSD(T) method is within 1 kcal mol⁻¹. Goldsmith et al.¹¹ proposed that the tunnelling correction and hindered rotor approximation are less accurate at lower temperature. Bugler et al.⁶⁷ studied reactions leading to cyclic ether formation and proposed that a factor of two may be assumed for uncertainties in harmonic vibrational frequencies and the anharmonicities of the 1-D hindered rotor mode. Jasper and Klippenstein^{44, 68} proposed that neglecting vibrational anharmonicity can be the dominant source of uncertainty in *a priori* predictions of thermochemistry and kinetics. At room temperature an error of just 150 cm⁻¹ in the threshold or reaction energy leads to an uncertainty of a factor of two in the computed rate coefficient or equilibrium constant.⁶⁹ Thus, in this work, two to three times uncertainty is expected in our theoretical calculations and hence the deviation between our calculation and experimental results are within the uncertainty.

○ Unimolecular reactions

1,3- $\dot{\text{C}}_5\text{H}_9$

The total pressure-dependent rate constants of 1,3- $\dot{\text{C}}_5\text{H}_9 \rightarrow$ all products are compared with the corresponding high-pressure limiting rate constants in Figure 16(a). At 1000 K, the fall-off of $k(1,3-\dot{\text{C}}_5\text{H}_9 \rightarrow \text{all})$ from the high-pressure limiting to 0.01 atm is less than a factor of two at temperatures below 800 K and increases to over two orders of magnitude at 1200 K.

At 10 atm, which is a frequently used condition in shock tube experiments, the fall-off compared with k_∞ can be more than an order of magnitude at temperatures above 1600 K. Hence, the total rate constants of the decomposition of $1,3\text{-}\dot{\text{C}}_5\text{H}_9$ show an obvious temperature- and pressure-dependence.

The branching ratios for the main products of $1,3\text{-}\dot{\text{C}}_5\text{H}_9$ radical decomposition are plotted in Figure 16(b). There is no significant pressure-dependence found for the branching ratios of these two dominant products, which is different with the phenomenon found for bimolecular reactions in our previous discussions. At low temperatures and different pressures, the formation of $2,5\text{-}\dot{\text{C}}_5\text{H}_9$ radical is the most favoured with the largest BR of $\sim 96\%$ at 400 K. The BRs of the $2,5\text{-}\dot{\text{C}}_5\text{H}_9$ radical decreases fast with increasing temperature and are overtaken by the formation of $1,3\text{-C}_4\text{H}_6 + \dot{\text{C}}\text{H}_3$ at temperatures around 650 K. At temperatures above 1000 K, over 87% of the products formed from $1,3\text{-}\dot{\text{C}}_5\text{H}_9$ radicals are $1,3\text{-C}_4\text{H}_6 + \dot{\text{C}}\text{H}_3$ radicals with the largest BR of 96.8%.

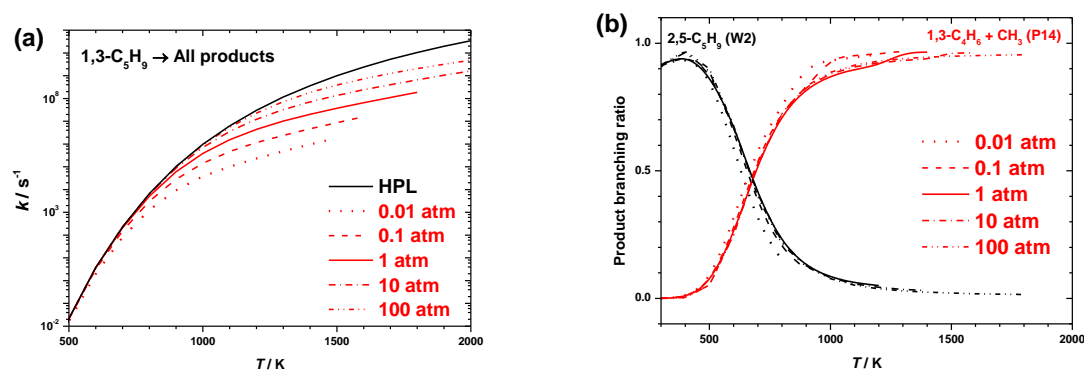


Figure 16. (a) The comparisons of pressure-dependent rate constants and high-pressure limiting rate constants for $1,3\text{-}\dot{\text{C}}_5\text{H}_9 \rightarrow$ all products as a function of temperature. (b) The branching ratios for main products from decomposition of $1,3\text{-}\dot{\text{C}}_5\text{H}_9$ radical at 0.01, 0.1, 1, 10 and 100 atm.

To validate our calculated rate constants, $k(1,3\text{-}\dot{\text{C}}_5\text{H}_9 \rightarrow 1,3\text{-C}_4\text{H}_6 + \dot{\text{C}}\text{H}_3)$ the high-pressure limiting rate constants and those at different pressures are compared with available literature studies in Figure 17. Wang et al.¹³⁻¹⁴ calculated the high-pressure limiting rate constants for this reaction using Quantum-Rice-Ramsperger-Kassel (QRRK) theory with species and TSs on the $\dot{\text{C}}_5\text{H}_9$ PES calculated at the CBS-QB3 level of theory. Baldwin and Walker's²¹ estimated the rate constants at 500 Torr based on their alkenes/ H_2/O_2 experimental results, and Perrin et al.²⁴ carried out measurement on the isomerisation reaction of 1- and 2-pentene and derived the rate constant for $1,3\text{-}\dot{\text{C}}_5\text{H}_9 \rightarrow 1,3\text{-C}_4\text{H}_6 + \dot{\text{C}}\text{H}_3$ in the pressure range

10–100 Torr. As shown in Figure 17, the k_∞ from Wang are 3.6 times faster than that calculated here at 1000 K and decrease to within 1.3 times difference at 2000 K. The difference at low temperatures possibly arises from the initial guess of A and E_a for the reverse reaction used in the QRRK calculation. Meanwhile, the rate constants at 0.01 atm from this work agree reasonably well with Perrin’s experimentally derived results at pressures in the range 0.01–0.13 atm with the differences being within 2.3–2.7 times. It is worth noting that the rate constant at 0.7 atm from Baldwin et al. tends to be too fast in comparison with this work and close to Wang’s high-pressure limiting rate constant.

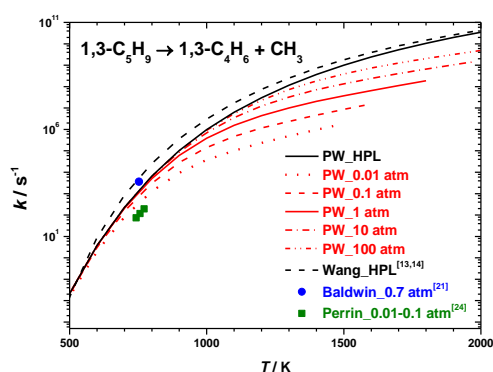


Figure 17. Rate constant comparisons for the β -scission reaction of 1,3- $\dot{\text{C}}_5\text{H}_9$ radical forming 1,3- $\text{C}_4\text{H}_6 + \dot{\text{C}}\text{H}_3$. The dashed lines represent the calculated results from Wang et al.¹³⁻¹⁴ at CBS-QB3 level of theory, the blue symbol represents Baldwin and Walker’s²¹ estimated result based on their alkenes/ H_2/O_2 experimental results, and the green symbols represent experimental results from Perrin et al.²⁴ over pressure range 10–100 Torr.

Wang et al.¹³⁻¹⁴ also have studied rate constants for 1,3- $\dot{\text{C}}_5\text{H}_9 \rightarrow 1,3\text{-C}_5\text{H}_8 + \dot{\text{H}}$ and 1,4- $\dot{\text{C}}_5\text{H}_9 \rightarrow \text{C}_3\text{H}_6 + \dot{\text{C}}_2\text{H}_3$, the rate constant comparisons of these two reactions are shown in Figure S5. The rate constants calculated in the present work agrees relatively well with Wang’s calculation for these two reactions with the values being within 1.3–3.5 times in the temperature range 300–2000 K.

1,4- $\dot{\text{C}}_5\text{H}_9$

The total pressure-dependent rate constants of 1,4- $\dot{\text{C}}_5\text{H}_9 \rightarrow$ all products are compared with the corresponding high-pressure limiting rate constants in Figure 18(a). The dominant products at low temperatures are methylenecyclopropylmethyl (W13, $\dot{\text{C}}\text{H}_2\text{-cyC}_3\text{H}_4\text{CH}_3$) and 3-methyl-1-buten-4-yl (W14, 3Me-1,4- $\dot{\text{C}}_4\text{H}_6$) formed via a low-energy barrier ring-opening reaction from W13. Due to $k(1,4\text{-}\dot{\text{C}}_5\text{H}_9 \rightarrow 3\text{Me-1,4-}\dot{\text{C}}_4\text{H}_6)$ and $k(1,4\text{-}\dot{\text{C}}_5\text{H}_9 \rightarrow \dot{\text{C}}\text{H}_2\text{-}$

cyC₃H₄CH₃) are not available over the entire temperature range, rate constants for these two channels are extrapolated to intermediate and/or high temperatures. It is shown that the fall-off of the total rate constants at 1700 K and 1 atm is over an order of magnitude, which indicates the significant pressure-dependence of the decomposition of 1,4-Ċ₅H₉ radical.

Based on calculated and extrapolated pressure-dependent rate constants, the branching ratios for important products produced from the decomposition of 1,4-Ċ₅H₉ radical are shown in Figure 18(b). At 1 atm, the formation of W14 is dominant with a BR over 80% at temperatures below 1100 K. Meanwhile, there is about 10%–20% W13 formed over the temperature range of 300–1400 K. As pressure increases, the formation of W14 at a specific temperature decreases until overtaken by the formation of W13 at 100 atm. There are also reasonable amounts (< 10%) of bimolecular products (1,3-C₄H₆ + ĊH₃) formed via the direct β-scission reaction of W14 and/or the chemically activated reaction at high temperatures. The total rate constant and branching ratio comparisons show the total rate constants have strong pressure-dependence and the product branching ratios are also sensitive to pressure and temperature.

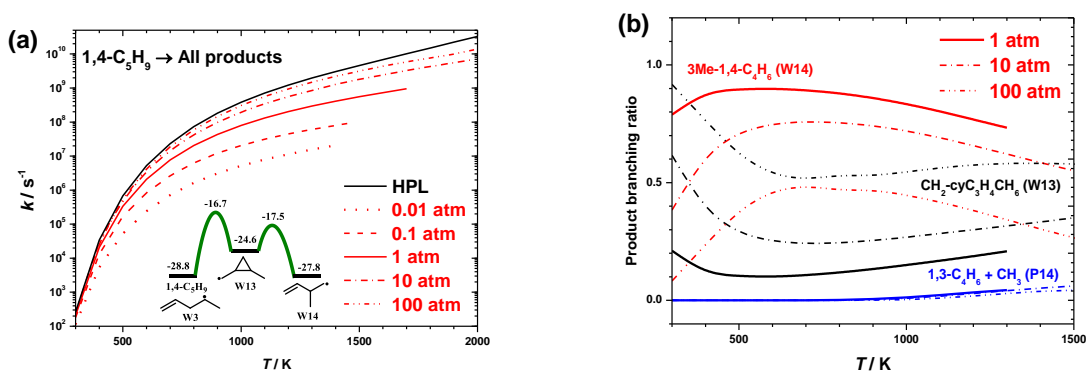


Figure 18. (a) The comparisons of pressure-dependent rate constants and high-pressure limiting rate constants for 1,4-Ċ₅H₉ → all products as a function of temperature. $k(1,4\text{-}\dot{\text{C}}_5\text{H}_9 \rightarrow 3\text{Me-1,4-}\dot{\text{C}}_4\text{H}_6)$ are extrapolated over a temperature range of 800–1400 K at 0.01 atm, 900–1500 K at 0.1 atm, 1100–1700 K at 1 atm, 1400–2000 K at 10 atm. $k(1,4\text{-}\dot{\text{C}}_5\text{H}_9 \rightarrow \dot{\text{C}}\text{H}_2\text{-cyC}_3\text{H}_4\text{CH}_3)$ are extrapolated over a temperature range of 600–1700 K at 1 atm, 700–2000 K at 10 atm and 900–2000 K at 10 atm. (b) The branching ratios for main products from decomposition of 1,4-Ċ₅H₉ radical at 0.01, 0.1, 1, 10 and 100 atm. The total rate constants are calculated with extrapolated $k(1,4\text{-}\dot{\text{C}}_5\text{H}_9 \rightarrow 3\text{Me-1,4-}\dot{\text{C}}_4\text{H}_6)$ and $k(1,4\text{-}\dot{\text{C}}_5\text{H}_9 \rightarrow \dot{\text{C}}\text{H}_2\text{-cyC}_3\text{H}_4\text{CH}_3)$, where no available rate constants exist.

1,5- \dot{C}_5H_9

The total pressure-dependent rate constants of $1,5-\dot{C}_5H_9 \rightarrow$ all products are compared with the corresponding high-pressure limiting rate constants in Figure 19(a). The fall-off in pressure-dependent rate constants compared with k_∞ can be up to two orders of magnitude at 1000 K and 0.01 atm, and ~ 7.6 times at 1500 K and 10 atm. Therefore, the total rate constants for the decomposition of $1,5-\dot{C}_5H_9$ radicals show an obvious pressure-dependence. The branching ratios for the dominant products generated from the decomposition of $1,5-\dot{C}_5H_9$ radical are shown in Figure 19(b). At 0.01 atm, the formation of cyclopentyl radical dominates at temperatures below 600 K until it is overtaken by the production of ethylene and allyl radicals. At 100 atm and low temperatures (< 500 K), about half of the reaction flux proceeds to form cyclopentyl radical with the other half forming methylenecyclobutyl radicals. The branching ratios of cyclopentyl and methylenecyclobutyl radicals have an obvious pressure-dependence at low temperatures, and their pressure-dependence diminishes gradually until it disappears at 1200 K. Meanwhile, the branching ratios of ethylene and allyl radical only show a pressure-dependence in the temperature range 500–1100 K. Hence, the pressure-dependent rate constants for the formation of ethylene and allyl radical should be considered in combustion mechanism development, and the pressure-dependent rate constants for the formation of cyclopentyl and methylenecyclobutyl radicals should also be included for simulations at temperatures below 1100 K.

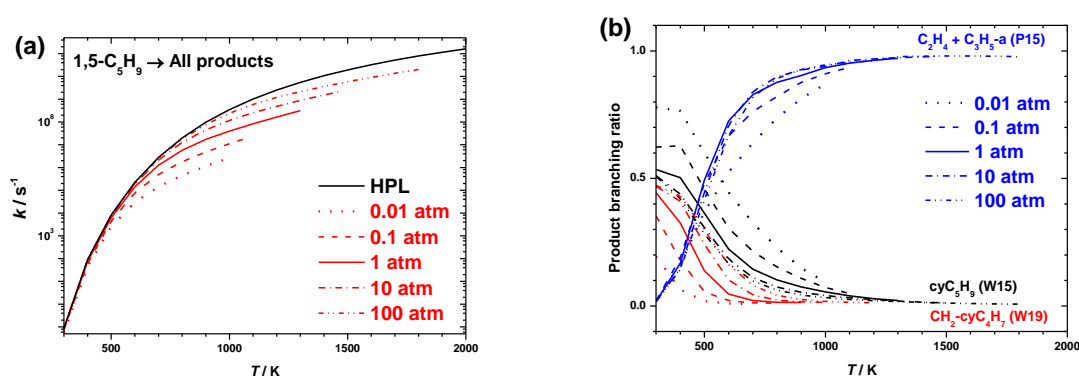


Figure 19. (a) The comparisons of pressure-dependent rate constants and high-pressure limiting rate constants for $1,5-\dot{C}_5H_9 \rightarrow$ all products as a function of temperature. (b) The branching ratios for main products from decomposition of $1,5-\dot{C}_5H_9$ radical at 0.01, 0.1, 1, 10 and 100 atm.

The β -scission reaction of $1,5-\dot{C}_5H_9$ to form ethylene + allyl radical has been studied by Tsang et al.⁸ and Awan et al.,¹² the comparison of the high-pressure limiting rate constants is

shown in Figure 20. Awan and co-workers¹² calculated the structural properties of radicals and stable species at the G3MP2B3 level of theory with a frequency scale factor of 0.96. Slight adjustments were made to the low frequency vibrations and reaction barriers to create a model that fitted their experimental data. They proposed that the standard uncertainties in the absolute rate constants are about a factor of 1.5 near 1000 K, increasing to a factor of two at 700 K and a factor of three at 1900 K. Tsang⁸ studied the decomposition and isomerization reactions of 1,5- \dot{C}_5H_9 radicals, estimating the energy barriers from available literature data. Rate constants were obtained by solving the Rice-Ramsperger-Kassel-Marcus (RRKM) and time-dependent Master Equation (ME). They proposed that breaking the allylic C–C bond to form allyl radicals and ethylene was the main reaction channel.⁸

The energy barriers for β -scission of the 1,5- \dot{C}_5H_9 radical are 21.6 kcal mol⁻¹ in this work, 19.9 kcal mol⁻¹ in Awan's work and 24.7 kcal mol⁻¹ in Tsang's work. The rate constants calculated in this work also lie between those proposed by Awan and Tsang corresponding to the trend in the energy barriers. The rate constants from Awan's work are 4.9 times higher than this work at 800 K and are 1.4 times higher at 1900 K. To test the influence of the different energy barriers, a calculation was carried out by replacing only the energy barrier in the current work to Awan's value. The rate constants calculated from this test are within 1.5 times of Awan's values in the temperature range 700–1900 K. Thus, the rate constant difference between this work and Awan's are mainly derived from the difference in energy barriers calculated at the different levels of theory and/or their adjustments in reaction barrier heights. Since the energies in this work are calculated at the ROCCSD(T) level of theory with the basis set extrapolated to aug-cc-pVQZ compared to the G3MP2B3 level used in Awan's work, **we believe our calculations to be more reliable**. Similarly, the rate constant difference between the present work and Tsang's study possibly arises from uncertainties in their A-factor estimations.

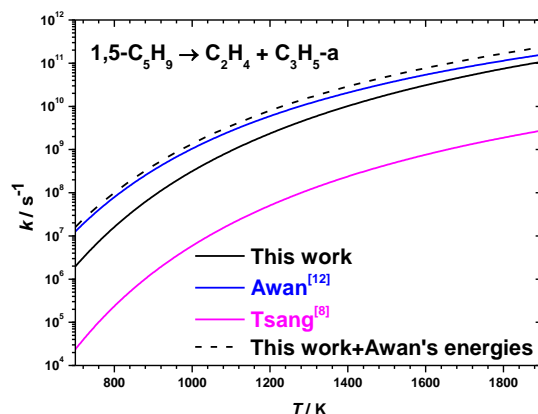


Figure 20. High-pressure limiting rate constants for β -scission reaction of 1,5- $\dot{\text{C}}_5\text{H}_9$ radical to allyl + ethylene. The blue line represents results calculated by Awan et al.¹² and the magenta line represents results calculated by Tsang et al.⁸.

Cyclopentyl radical reactions

The total pressure-dependent rate constants of $\text{cy}\dot{\text{C}}_5\text{H}_9 \rightarrow$ all products are compared with the corresponding high-pressure limiting rate constants in Figure 21(a). Similar to the other $\dot{\text{C}}_5\text{H}_9$ radicals, the total rate constants for the decomposition of $\text{cy}\dot{\text{C}}_5\text{H}_9$ radicals show an obvious temperature- and pressure-dependence. The fall-off can be up to two orders of magnitude at 0.01 atm and over an order of magnitude at 10 atm. The branching ratios for the dominant products generated from the decomposition of $\text{cy}\dot{\text{C}}_5\text{H}_9$ radical are shown in Figure 21(b). At 300 K, approximately 86.4% of $\text{cy}\dot{\text{C}}_5\text{H}_9$ radicals lead to 1,5- $\dot{\text{C}}_5\text{H}_9$ radicals, with 13.6% decomposing to $\text{cyC}_5\text{H}_8 + \dot{\text{H}}$ atoms. As temperature increases, the BR leading to 1,5- $\dot{\text{C}}_5\text{H}_9$ radicals decreases rapidly and becomes undefinable, when well-skipping occurs and the chemically activated reactions forming bimolecular products start to dominant. The importance of $\text{C}_2\text{H}_4 + \dot{\text{C}}_3\text{H}_5\text{-a}$ formation decreases with increasing pressure while the formation of $\text{cyC}_5\text{H}_8 + \dot{\text{H}}$ only shows a slight positive pressure-dependence. The $\text{BR}(\text{C}_2\text{H}_4 + \dot{\text{C}}_3\text{H}_5\text{-a})/\text{BR}(\text{cyC}_5\text{H}_8 + \dot{\text{H}})$ ratios are shown to be temperature- and pressure-dependent and are very important in the simulation of cyC_5H_8 and $\text{cyC}_5\text{H}_{10}$ profiles.

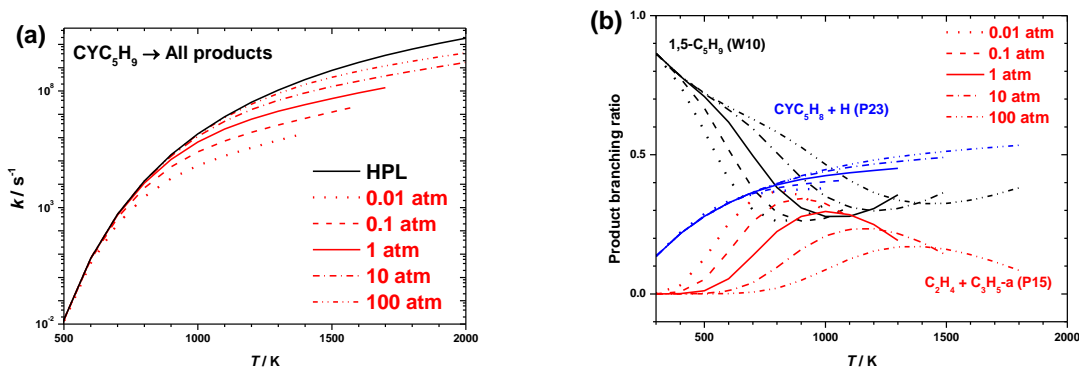


Figure 21. (a) The comparisons of pressure-dependent rate constants and high-pressure limiting rate constants for $\text{cy}\dot{\text{C}}_5\text{H}_9 \rightarrow$ all products as a function of temperature. (b) The branching ratios for main products from decomposition of $\text{cy}\dot{\text{C}}_5\text{H}_9$ radical at 0.01, 0.1, 1, 10 and 100 atm.

As described in previously, Tsang⁸ calculated the high-pressure limiting rate constants for the decomposition reactions of $1,5\text{-}\dot{\text{C}}_5\text{H}_9$ with energy barriers estimated from available literature data at that time. Sirjean et al.¹⁰ calculated the high-pressure limiting rate constants for cyclization reaction of $1,5\text{-}\dot{\text{C}}_5\text{H}_9$ at the CBS-QB3 level of theory using classical TST in the temperature range 500–2000 K. Wang et al.^{13–14} studied reactions related to $1,5\text{-}\dot{\text{C}}_5\text{H}_9$ on the $\dot{\text{C}}_5\text{H}_9$ PES using the CBS-QB3 composite method. Pressure-dependent rate constants were calculated using Quantum-Rice-Ramsperger-Kassel (QRRK) theory and k_∞ were calculated from CBS-QB3 calculations or were estimated based on reaction rate rules. Al Rashidi and co-workers¹⁵ studied the C–C and C–H β -scission at the UCCSD(T)-F12b/cc-pVTZ-F12//M06-2X/6-311++G(d,p) level of theory and calculated high-pressure limiting rate constants. Awan and co-workers^{12, 16} calculated the rate constants for $\text{cy}\dot{\text{C}}_5\text{H}_9$ decomposition reactions using a combination of RRKM/ME calculations and the derived product ratio from their shock tube experiment for $\text{cy}\dot{\text{C}}_5\text{H}_9$ decomposition.

Gordon¹⁷ measured the $k(\dot{\text{C}}\text{D}_3 + \text{cyC}_5\text{H}_{10} \rightarrow \text{CD}_3\text{H} + \text{cy}\dot{\text{C}}_5\text{H}_9) \cdot k(\text{cy}\dot{\text{C}}_5\text{H}_9 \rightarrow \text{C}_2\text{H}_4 + \dot{\text{C}}_3\text{H}_5\text{-a}) / k(\dot{\text{C}}\text{D}_3 + \text{cy}\dot{\text{C}}_5\text{H}_9 \rightarrow \text{CH}_3\text{-cy}\dot{\text{C}}_5\text{H}_9)$ ratios by studying the photolysis of cyclopentane–acetone mixtures between 580–680 K at pressures in the range 0.05–0.06 bar. The ratios were derived from product yields and the pre-exponential factor (A) and the activation energy (E_a) for $\text{cy}\dot{\text{C}}_5\text{H}_9 \rightarrow \text{C}_3\text{H}_5\text{-a} + \text{C}_2\text{H}_4$ were derived with reasonable A and E_a values for the other two reactions obtained from the literature. Headford-Styring and Walker²⁶ studied the oxidation of cyclopentane by adding cyclopentane to $\text{H}_2\text{-O}_2$ mixtures in the temperature range 673–783 K at 500 Torr. The $k(\text{cy}\dot{\text{C}}_5\text{H}_9 \rightarrow 1,5\text{-}\dot{\text{C}}_5\text{H}_9)$ was considered as the rate determining step for the

production of $C_2H_4 + \dot{C}_3H_5\text{-a}$ and was determined by the yields of ethylene. They also reinterpreted Gordon's data with new rate constants for $CD_3 + cyC_5H_{10} \rightarrow CD_3H + cy\dot{C}_5H_9$ and $CD_3 + cy\dot{C}_5H_9 \rightarrow CH_3\text{-}cy\dot{C}_5H_9$ which are plotted as revised data in Figure 22(a).

The k_∞ comparisons between this work and the literature data for $cy\dot{C}_5H_9$ decomposition reactions are shown in Figure 22. For $cy\dot{C}_5H_9 \rightarrow cyC_5H_8 + \dot{H}$ large discrepancies are observed among the different literature values (e.g. the difference between the rate constants of Sirjean and Tsang is about a factor of 50 at 2000 K). These large discrepancies are mainly due to three reasons: (1) different level of theories used in the quantum calculations; (2) different software employed in rate constant calculations; (3) empirical adjustments for the frequencies and energy barriers. At temperatures above 1200 K, the trend of k_∞ for this channel is: $k_\infty(\text{Tsang}) < k_\infty(\text{This work}) < k_\infty(\text{Al Rashidi}) < k_\infty(\text{Awan}) < k_\infty(\text{Sirjean})$. The k_∞ calculated here agrees well with Al Rashidi's high-level calculation, with both values being within 40% of one another in the temperature range 700–2000 K. For pressure-dependent rate constants, the values calculated here are compared with available experimental data as presented in Figure 22(a). Headford-Styring and Walker²⁶ carried out measurements at 0.67 atm and our results, calculated at 1.0 atm agrees very well with theirs. The revised Gordon's results also show good agreement with Headford-Styring and this work at low temperatures where the rate constants show no obvious fall-off.

For $cy\dot{C}_5H_9 \rightarrow 1,5\text{-}\dot{C}_5H_9$ shown in Figure 22(b), the largest discrepancy in the literature data is a factor of 15 over the entire temperature range. The trend of k_∞ at 1000–2000 K is: $k_\infty(\text{Tsang}) < k_\infty(\text{This work}) \approx k_\infty(\text{Al Rashidi}) < k_\infty(\text{Wang}) < k_\infty(\text{Awan}) < k_\infty(\text{Sirjean})$. The k_∞ of Sirjean are similar to those of Awan and are consistently over eight times faster than our calculations. Wang and Sirjean both used the CBS-QB3 level of theory for optimizations and energy calculations, the difference for k_∞ calculated from these two studies is less than a factor of two over the entire temperature range. Similar to $cy\dot{C}_5H_9 \rightarrow cyC_5H_8 + \dot{H}$, the k_∞ for the ring-opening reaction in the present work agree very well with those presented by Al Rashidi et al.,¹⁵ being within 20% of one another in the temperature range 700–2000 K. Al Rashidi et al.¹⁵ simulated the combustion of cyC_5H_{10} in a JSR and found that the better fits to the concentration profiles of cyC_5H_{10} in the experiments were obtained using their rate constants compared with the literature data. In addition, $k(cy\dot{C}_5H_9 \rightarrow 1,5\text{-}\dot{C}_5H_9)$ measured in Headford-Styring's experiment agree very well with our results at 1 atm. Hence, we believe that the high-pressure limiting rate constants for $cy\dot{C}_5H_9$ radical decomposition calculated in this work should be reliable.

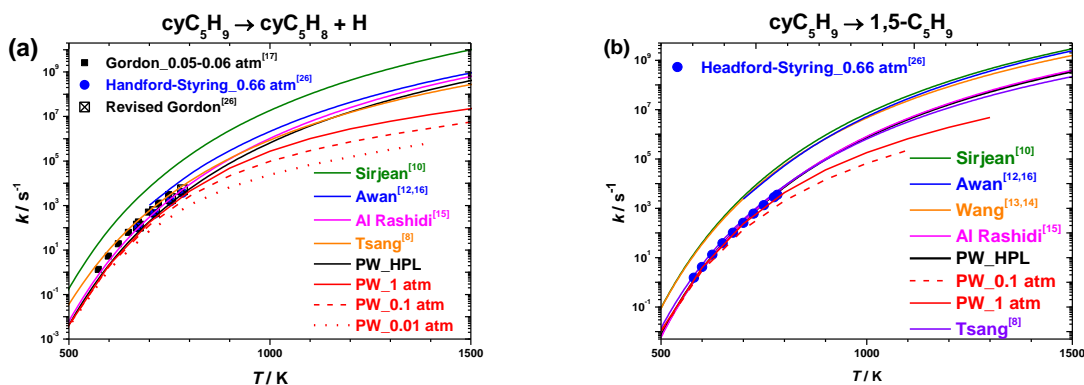


Figure 22. Rate constants for (a) C–H β -scission reaction of $\text{cy}\dot{\text{C}}_5\text{H}_9$ radicals forming $\text{cyC}_5\text{H}_8 + \dot{\text{H}}$, (b) C–C β -scission reaction of $\text{cy}\dot{\text{C}}_5\text{H}_9$ radicals forming $1,5\text{-}\dot{\text{C}}_5\text{H}_9$. The green, blue, orange, red and magenta lines represent results calculated by Sirjean et al.,¹⁰ Awan et al.,^{12, 16} Wang et al.,¹³⁻¹⁴ Al Rashidi et al.,¹⁵ and Tsang et al.,⁸ respectively. The symbols stand for different results derived from experiments: \blacksquare Gordon,¹⁷ \bullet Handford-Styring,²⁶ \boxtimes revised values of Gordon’s work by Handford-Styring.²⁶

Al Rashidi and co-workers¹⁵ carried out the identification and quantification of species generated during the oxidation of $\text{cyC}_5\text{H}_{10}$ in a JSR. They conducted sensitivity and reaction path analyses and found that the reactivity of cyC_5H_8 was highly sensitive to the C–C/C–H scission branching ratio of $\text{cy}\dot{\text{C}}_5\text{H}_9$ radical decomposition. The high-pressure limiting branching ratio for $\text{cy}\dot{\text{C}}_5\text{H}_9$ decomposition were compared with theoretical results from the literature in the temperature range 900–1200 K. The branching ratios from Awan,¹² this work, Al Rashidi,¹⁵ Tsang⁸ and Sirjean¹⁰ at 1000 K are 3.46, 1.22, 0.84, 0.78 and 0.39, respectively. What stands out is that these high-pressure limiting branching ratios indicate the k_∞ for the ring-opening reaction (C–C β -scission) is similar or even slower than that for the C–H β -scission reaction excluding Awan’s result, which is 8.8 times larger than that of Sirjean. It is noticeable that the deviations in branching ratios between this work and those of Al Rashidi and Tsang are within 50%. The C–C/C–H high-pressure limiting branching ratio in Awan’s work were derived from the experimental yields of C_2H_4 and cyC_5H_8 ,¹² with slight adjustments for low frequency vibrations in the TSs and small empirical changes in reaction barriers to fit their experimental data. As suggested by Manion and Awan,^{12, 16} the discrepancies in branching ratios between the experiments and theoretical calculations for $\text{cy}\dot{\text{C}}_5\text{H}_9$ radical decomposition show the difficulties in precisely predicting branching ratios when two competitive channels have similar rate constants. In addition, it is also possible that the additives (species used as $\dot{\text{H}}$ source, radical scavenger), which are used in large amounts

in the experiment, and their decomposition products may react with $\text{cyC}_5\text{H}_{10}$ or with the intermediates to influence the formation/consumption of cyC_5H_8 . Hence, to obtain accurate branching ratios for cyC_5H_9 radical decomposition, more high-level theoretical calculations and benchmarking experimental measurements are needed. The species profiles for Manion's $\text{cyC}_5\text{H}_{10} + \dot{\text{H}}$ experiments are simulated with our model and the chemistry is discussed in detail in Section 3.4.2.

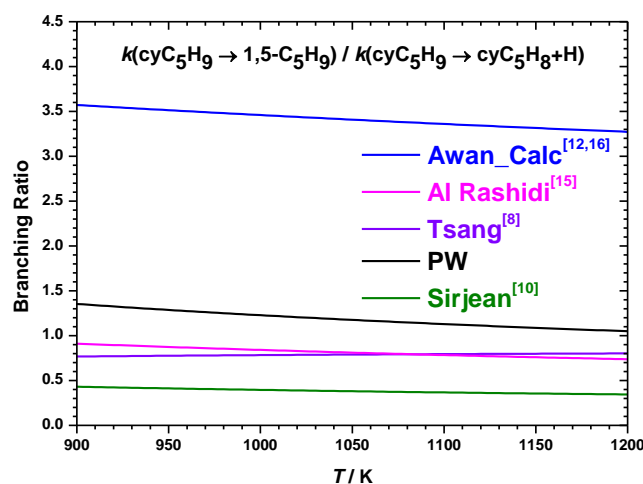


Figure 23. The branching ratios of cyC_5H_9 radicals comparing with high-pressure limiting rate constants in the literature. The blue, red, magenta and green lines represent results calculated by Awan et al.,^{12, 16} Al Rashidi et al.,¹⁵ Tsang et al.,⁸ and Sirjean et al.,¹⁰ respectively.

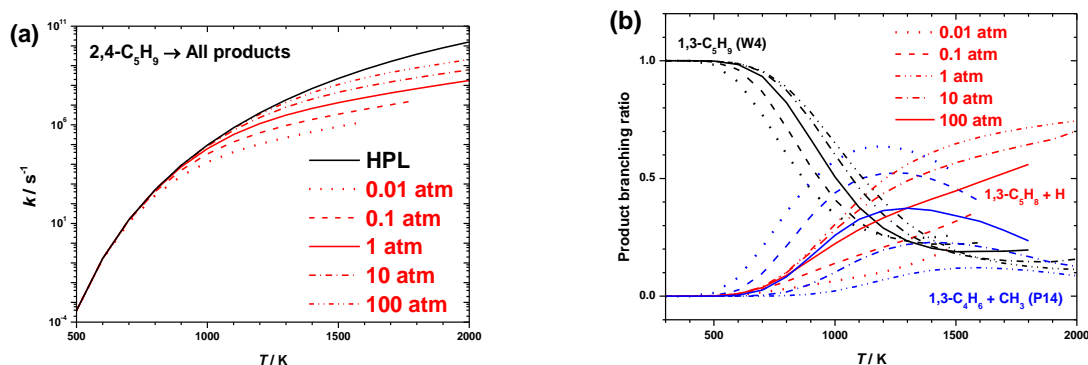


Figure 24. (a) The comparisons of pressure-dependent rate constants and high-pressure limiting rate constants for $2,4\text{-C}_5\text{H}_9 \rightarrow$ all products as a function of temperature. (b) The branching ratios for main products from decomposition of $2,4\text{-C}_5\text{H}_9$ radical at 0.01, 0.1, 1, 10 and 100 atm.

2,4- \dot{C}_5H_9

As shown in Figure 24(a), the total pressure-dependent rate constants of 2,4- $\dot{C}_5H_9 \rightarrow$ all products are compared with the corresponding high-pressure limiting rate constants showing significant fall-off with a largest fall-off of over two order of magnitude at 0.01 atm and 1500 K. At low temperatures (< 700 K) shown in Figure 24(b), over 90% of 2,4- \dot{C}_5H_9 radicals undergo isomerisation to form 1,3- \dot{C}_5H_9 radicals, and as temperature increases, the production of 1,3- $C_4H_6 + \dot{C}H_3$ is preferred at low pressures and the production of 1,3- $C_5H_8 + \dot{H}$ is preferred at high pressures. The branching ratios of bimolecular products generated from the decomposition of 2,4- \dot{C}_5H_9 radicals are temperature- and pressure-dependent which should be considered in species profile simulations.

2,5- \dot{C}_5H_9

The total pressure-dependent rate constants of 2,5- $\dot{C}_5H_9 \rightarrow$ all products are compared with the corresponding high-pressure limiting rate constants in Figure 25(a). The rate constants for dominant channel 2,5- $\dot{C}_5H_9 \rightarrow$ sec-ethyl-cyclopropane (W6, $CH_3\dot{C}H-cyC_3H_5$) become undefinable at relatively low temperatures compared with other \dot{C}_5H_9 radicals, which suggests the rate constant calculations for reactions related to 2,5- \dot{C}_5H_9 radical are more difficult. The rate constants for this channel are extrapolated to intermediate and/or high temperatures, then the total rate constants and branching ratios are calculated. Similar to the other \dot{C}_5H_9 radicals, the total rate constants for the decomposition of 2,5- \dot{C}_5H_9 radical show obvious fall-off at high temperatures, and the fall-off at 10 atm can reach up to an order of magnitude.

The BRs of dominant products generated from the decomposition of 2,5- \dot{C}_5H_9 radical are shown in Figure 25(b). At low temperatures and high pressures, the ring-formation channel forming sec-ethyl-cyclopropane ($CH_3\dot{C}H-cyC_3H_5$) radical with a low-energy barrier is dominant. However, as illustrated in Part I, there are no subsequent reactions of sec-ethyl-cyclopropane radicals which have energy barriers lower than the reverse reaction of its formation. Meanwhile, at low pressures, the formation of 1,3- \dot{C}_5H_9 radical is also significant with a maximum BR over 40% at 0.01 atm. 1,3- \dot{C}_5H_9 radical is formed via a chemically activated reaction, which contributes to the formation of 1,3- $C_4H_6 + \dot{C}H_3$ via direct β -scission reaction. As one might anticipate, the BRs of $CH_3\dot{C}H-cyC_3H_5$ radical increases as pressure increases and the BR(1,3- \dot{C}_5H_9) decreases as pressure increases due to their competition. The BRs of 1,3- $C_4H_6 + \dot{C}H_3$ increases as temperature increases and decreases with increasing pressure, and there are certain amounts of the other bimolecular products formed at high

temperatures and high pressures. The obvious pressure-dependence of the BRs indicates the importance of pressure-dependent rate constants on product predictions.

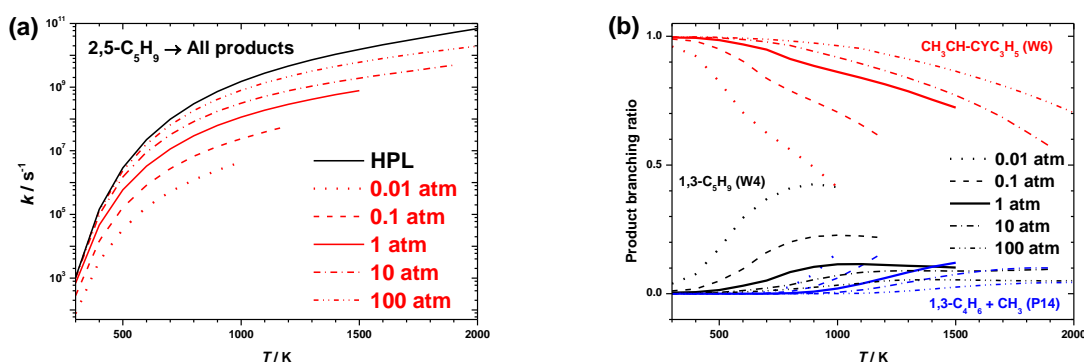


Figure 25. (a) The comparisons of pressure-dependent rate constants and high-pressure limiting rate constants for $2,5\text{-}\dot{\text{C}}_5\text{H}_9 \rightarrow$ all products as a function of temperature. $k(2,5\text{-}\dot{\text{C}}_5\text{H}_9 \rightarrow \text{CH}_3\dot{\text{C}}\text{H-cyC}_3\text{H}_5)$ are extrapolated over a temperature range of 600–1000 K at 0.01 atm, 700–1200 K at 0.1 atm, 800–1500 K at 1 atm, 900–1900 K at 10 atm. (b) The branching ratios for main products from decomposition of $2,5\text{-}\dot{\text{C}}_5\text{H}_9$ radical at 0.01, 0.1, 1, 10 and 100 atm, with $k(2,5\text{-}\dot{\text{C}}_5\text{H}_9 \rightarrow \text{CH}_3\dot{\text{C}}\text{H-cyC}_3\text{H}_5)$ extrapolated where no available rate constants exist.

- **Chemical kinetic modeling**

The chemical kinetic model with pressure-dependent rate constants have been used for homogenous batch reactor simulations and the species profiles for different wells and products are compared with available experimental results to analyse and validate the chemistry of $\dot{\text{C}}_5\text{H}_9$ radicals at different temperatures and pressures.

Awan et al.¹² performed single-pulse shock tube experiments to study the thermal decomposition of cyclopentyl radical in the temperature range 950–1116 K at pressures of 2.3–3.4 bar. Cyclopentyl radicals were generated by H-atom abstraction from cyclopentane by $\dot{\text{H}}$ atoms, which were produced by the decomposition of hexamethylethane (HME). 1,3,5-trimethylbenzene (T135MB) was used as both a rate reference for $\dot{\text{H}}$ atom reactions and as a radical scavenger. The reverse Diels-Alder reaction of 4-vinylcyclohexene (VCH) which produces 1,3-butadiene was used as a standard reaction, and the shock temperatures were determined by following the progression of this reaction which had a known rate constant. In 2018, Manion and Awan studied $\dot{\text{H}}$ atom addition to cyclopentene in a single pulse shock tube at 863–1167 K and 160–370 kPa.¹⁶ HME was used a $\dot{\text{H}}$ atom source and T135MB as a radical scavenger for three mixtures at temperatures above 1000 K.

To simulate their experiments, the rate constants for reactions related to these additives and the thermochemistry for them and their related species are included in our model which is described in detail in Section 2.2 below. The closed homogeneous batch reactor model in Chemkin-Pro is used to predict the mole fractions of different products generated from cyclopentane + $\dot{\text{H}}$ and cyclopentene + $\dot{\text{H}}$. Five mixtures in total (two for $\text{cyC}_5\text{H}_{10}$ + $\dot{\text{H}}$ and three for cyC_5H_8 + $\dot{\text{H}}$) containing HME and 135TMB fuels are simulated at experimental conditions and the comparison results are shown in Figures. 26–28. For each experiment, Mixture A has been measured over a wide temperature range, while there are only a few data points measured for Mixtures B and C. To simplify the plots, the experimental data points for Mixtures B and C are plotted as open/crossed symbols, and their corresponding simulated concentrations are plotted together with Mixture A as outstanding points.

Cyclopentane + $\dot{\text{H}}$ \rightarrow different products

For the cyclopentane + $\dot{\text{H}}$ experiments, no concentration profiles of the reactants are provided in Manion's paper.¹⁶ Hence, only the concentration profiles for different products generated from the reactions of $\text{cyC}_5\text{H}_{10}$, HME, T135MB and VCH are simulated and analysed. For mixtures A and B used in the experiments, the main difference is the use of T135MB as a radical scavenger in Mixture A and not in Mixture B.

As shown in Figure 26, the concentration profiles of isobutene, which is generated via $\text{HME} \rightarrow 2\dot{\text{C}}_4\text{H}_9\text{-I} \rightarrow 2\text{C}_4\text{H}_8\text{-I} + 2\dot{\text{H}}$, is very well predicted by our model, indicating the accurate prediction of the generation of $\dot{\text{H}}$ atoms. Meanwhile, the prediction of $[\text{C}_2\text{H}_4]$ agrees very well with the experiment, which are mostly produced together with allyl radicals via the decomposition of 1,5- $\dot{\text{C}}_5\text{H}_9$ radicals and also via chemically activated reactions from $\text{cy}\dot{\text{C}}_5\text{H}_9$ radicals. $\text{cy}\dot{\text{C}}_5\text{H}_9$ radicals are generated by H-atom abstraction reactions from $\text{cyC}_5\text{H}_{10}$ by $\dot{\text{H}}$ atoms produced from HME decomposition, and also by other radicals such as $\dot{\text{C}}\text{H}_3$, $\dot{\text{C}}_2\text{H}_3$, $\dot{\text{C}}_3\text{H}_5\text{-a}$, etc. The predicted concentrations of cyC_5H_8 for Mixture A are about 3.2–2.1 times larger than the experimental results in the temperature range 950–1012 K and are 2.0–1.7 times larger at temperatures above 1012 K. However, the predicted concentrations of cyC_5H_8 for Mixture B, which doesn't contain T135MB as a radical scavenger, are within 50% of the experimental results. Therefore, we suggest the T135MB chemistry sub-mechanism can influence the prediction of cyC_5H_8 in the $\text{cyC}_5\text{H}_{10}$ /HME/VCH experiments. Due to the complexity of the decomposition mechanism of T135MB, the detailed chemistry of the influence of T135MB on the production of cyC_5H_8 is still unclear.

Using the current model, we are able to predict [1,3-dimethylbenzene (D13MB)], [1-ethyl-3,5-dimethylbenzene (D35MBC₂H₅)] very well, and within a factor of two when [1-butenyl-3,5-dimethylbenzene (D35MBC₄H₇)] are larger than 1 μL/L. D35MBC₂H₅ and D35MBC₄H₇ are the recombination products of 1-methylene-3,5-dimethylbenzene (D35MBC \dot{C} H₂) radicals with methyl and allyl radicals, respectively. In addition, the other important products in order of decreasing concentration are 1,5-hexadiene, methane and propene, and there are also small amounts (< 5 μL/L) of ethane, allene, cyclopropane, cyclopentadiene (C₅H₆) and 1-pentene formed, for which the current model can provide good predictions.

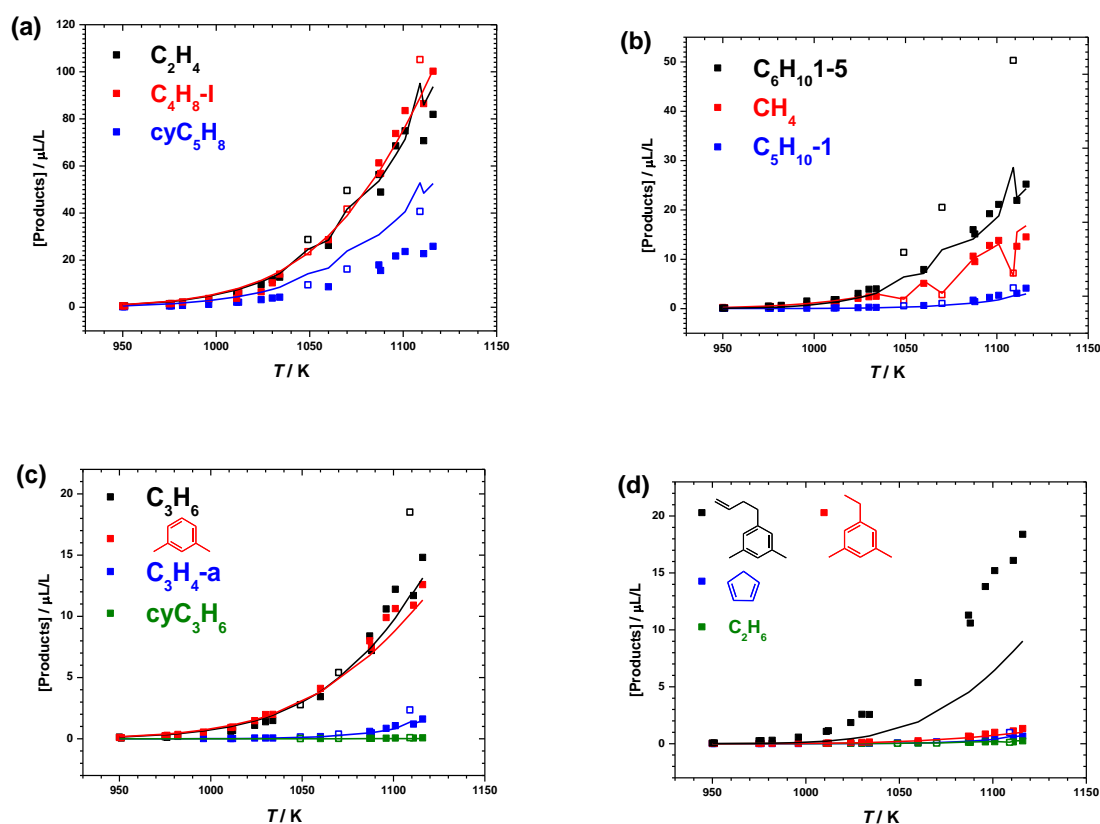


Figure 26. Experimental (symbols)¹² and modelled (lines) concentration profiles for products generated from \dot{H} atoms addition to cyclopentane at temperatures over 950–1116 K and pressures of 2.3–3.4. The solid symbols represent product concentration profiles for Mixture A which contains 110 μL/L HME, 20700 μL/L cyC₅H₁₀, 100 μL/L VCH and 6500 μL/L T135MB in Argon. The results shown as open symbols are for Mixture B which contains 110 μL/L HME, 23000 μL/L cyC₅H₁₀ and 100 μL/L VCH in Argon. Experiments were configured to have reaction times of 500±50 μs and the concentration profiles are simulated with same reaction times.

Cyclopentene + $\dot{\text{H}}$ \rightarrow different products

To validate the reliability of our calculations, the same chemical kinetic model has been used to simulate the species profiles of the $\text{cyC}_5\text{H}_8 + \dot{\text{H}}$ experiments. For the sing-pulse shock tube experiments the product concentrations were based on FID analyses, with MS used to identify the products. Including possible systematic errors, the analytical uncertainty (1σ) for the main products was estimated to be about 3%. Since large amounts of cyC_5H_8 and T135MB are used in this experiment and small amounts of HME used as the $\dot{\text{H}}$ atom source, the consumptions of cyC_5H_8 and T135MB are relatively small compared with their initial concentrations. Hence, the absolute analytical uncertainties for the measurements of $[\text{cyC}_5\text{H}_8]$ and $[\text{T135MB}]$ can be up to $\sim 500 \mu\text{L/L}$ based on their large concentrations. As a result, the measured concentrations of cyC_5H_8 and T135MB can sometimes be larger than their initial concentrations, as shown in Figure 27. We also see that our model is able to reproduce the consumption of the three reactants used in the experiments, especially the [HME] which has a smaller absolute analytical uncertainty.

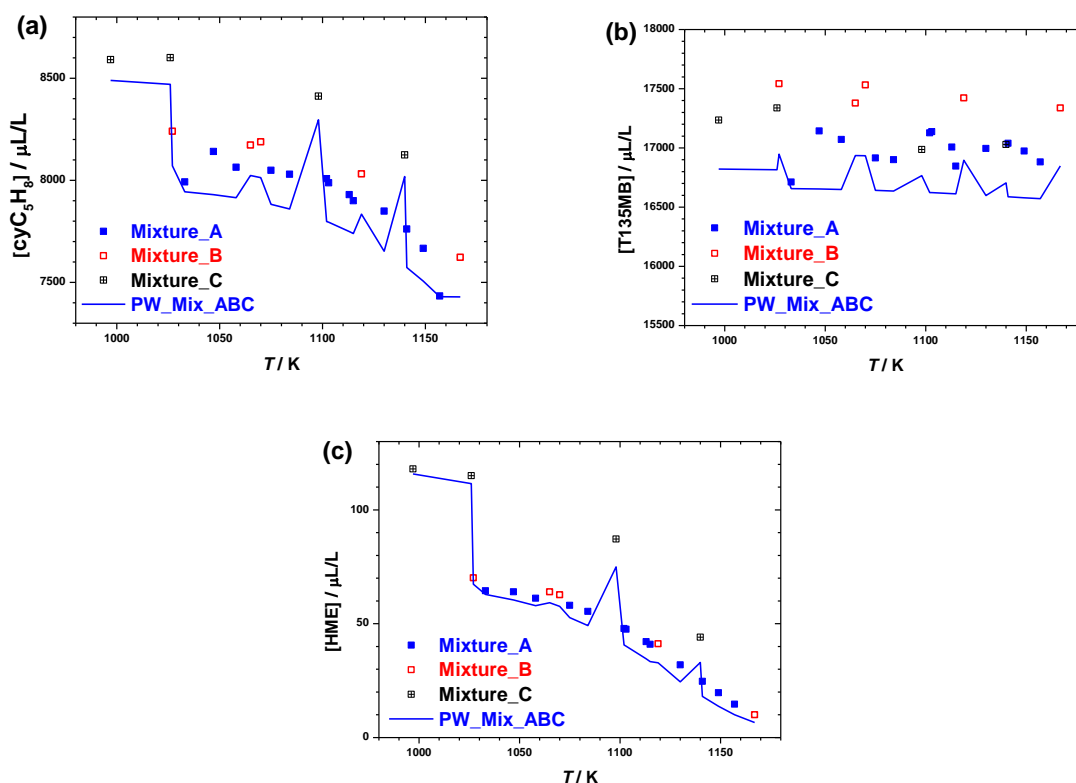


Figure 27. Experimental (symbols)¹⁶ and modelled (lines) concentration profiles for reactants used in experimental studies for $\dot{\text{H}}$ atom addition to cyclopentene at temperatures over 997–1167 K and pressures at 2.6–3.7 bar. The solid lines represent the predictions by our model for three mixtures. The initial compositions for three mixtures are: (A) 68 $\mu\text{L/L}$ HME, 7972

$\mu\text{L/L}$ cyC_5H_8 , 16659 $\mu\text{L/L}$ T135MB; (B) 72 $\mu\text{L/L}$ HME, 8098 $\mu\text{L/L}$ cyC_5H_8 , 16957 $\mu\text{L/L}$ T135MB; (C) 119 $\mu\text{L/L}$ HME, 8507 $\mu\text{L/L}$ cyC_5H_8 , 16834 $\mu\text{L/L}$ T135MB, in Argon. The concentration profiles in experiments and simulations are configured to have reaction times of $500 \pm 50 \mu\text{s}$.

The concentration profiles for the products generated in the $\text{cyC}_5\text{H}_8 + \dot{\text{H}}$ experiments are shown in Figure 28. What stands out in this figure is the existence of outlier data points for several species. For instance, the initial concentration of HME of Mixture C is higher than that of Mixture A and there are enough cyC_5H_8 in both systems, resulting in more $\dot{\text{H}}$ atoms generated which should increase the reaction reactivity and intermediates formation, such as allyl radicals. The concentrations of 1,5- C_6H_{10} predicted for Mixture C (which can be formed by allyl radical recombination) are shown to be higher than concentrations measured for Mixture A at similar temperatures, excluding one point at 1140 K which is \sim a factor of two smaller than that for Mixture A at 1141 K. A similar phenomenon is found for [1- C_4H_8] of Mixture C at 1098 K and 1140 K. These outliers are neglected in deviation discussion below to reasonably validate the performance of the model.

Similar to the $\text{cyC}_5\text{H}_{10} + \dot{\text{H}}$ experiment, HME decomposition and the formation of isobutene indicate the production of $\dot{\text{H}}$ atoms in the system, which can be quantitatively predicted by our model. In addition, the quantity of ethylene, as the most important product produced from $\text{cyC}_5\text{H}_8 + \dot{\text{H}}$, is well predicted with the deviations being within 50%. The accurate prediction of [C_2H_4] in Figure 28(a) suggests the chemistry in our model including $\text{cyC}_5\text{H}_8 + \dot{\text{H}} \rightarrow \text{cy}\dot{\text{C}}_5\text{H}_9 \rightarrow 1,5\text{-}\dot{\text{C}}_5\text{H}_9$, the following β -scission reactions of 1,5- $\dot{\text{C}}_5\text{H}_9$ radicals, and also the chemically activated reactions from the intermediates on $\dot{\text{C}}_5\text{H}_9$ PES to produce $\text{C}_2\text{H}_4 + \dot{\text{C}}_3\text{H}_5$ -a are reasonable. The current model can also predict the formation and consumption of different intermediates: (1) $\dot{\text{C}}\text{H}_3$ radicals, which are mainly formed through $\text{T135MB} + \dot{\text{H}} \rightarrow \text{D13MB} + \dot{\text{C}}\text{H}_3$, and about 10% are formed via decomposition reactions of iso-butyl/tert-butyl radicals to produce $\text{C}_3\text{H}_6 + \dot{\text{C}}\text{H}_3$. The dominant product from $\dot{\text{C}}\text{H}_3$ radicals is CH_4 produced via H-atom abstraction reactions from T135MB by $\dot{\text{C}}\text{H}_3$, whose concentrations are predicted with deviations within 50%. There is also a small amount of C_2H_6 ($< 0.4 \mu\text{L/L}$) formed through the self-recombination of $\dot{\text{C}}\text{H}_3$ radicals, and the predicted concentrations agree with the measurements within a factor of two. (2) iso-butyl/tert-butyl radicals, the consumption of butyl radicals can be validated based on the good predictions of [C_4H_8 -I], [C_3H_6] and [CH_4]. (3) 1,3-pentadien-5-yl radicals (the dominant products of H-atom abstraction reactions of 1,3- and 1,4-pentadiene), [C_2H_2] can be predicted with deviations

within a factor of two indicating the formation of 1,3-pentadien-5-yl radicals and the decomposition pathway to form \dot{C}_3H_5 -a + C_2H_2 are well described in our model. (4) allyl radicals are the key intermediates for the formations of allene, 1-butene, 1,5-hexadiene and D35MBC₄H₇ (recombination products of allyl and D35MB $\dot{C}H_2$ radicals). [C₃H₄-a] formed via the decomposition of allyl radicals are predicted within 50% when [C₃H₄-a] > 0.5 μ L/L. [C₄H₈-1] formed via the recombination of allyl and methyl radicals can be relatively well predicted at temperatures below 1130 K and is less than 87% under-predicted at higher temperatures. 1,5-C₆H₁₀, which is mainly formed through the recombination of allyl radicals, can be predicted by the current model, with a largest deviation of a factor of two.

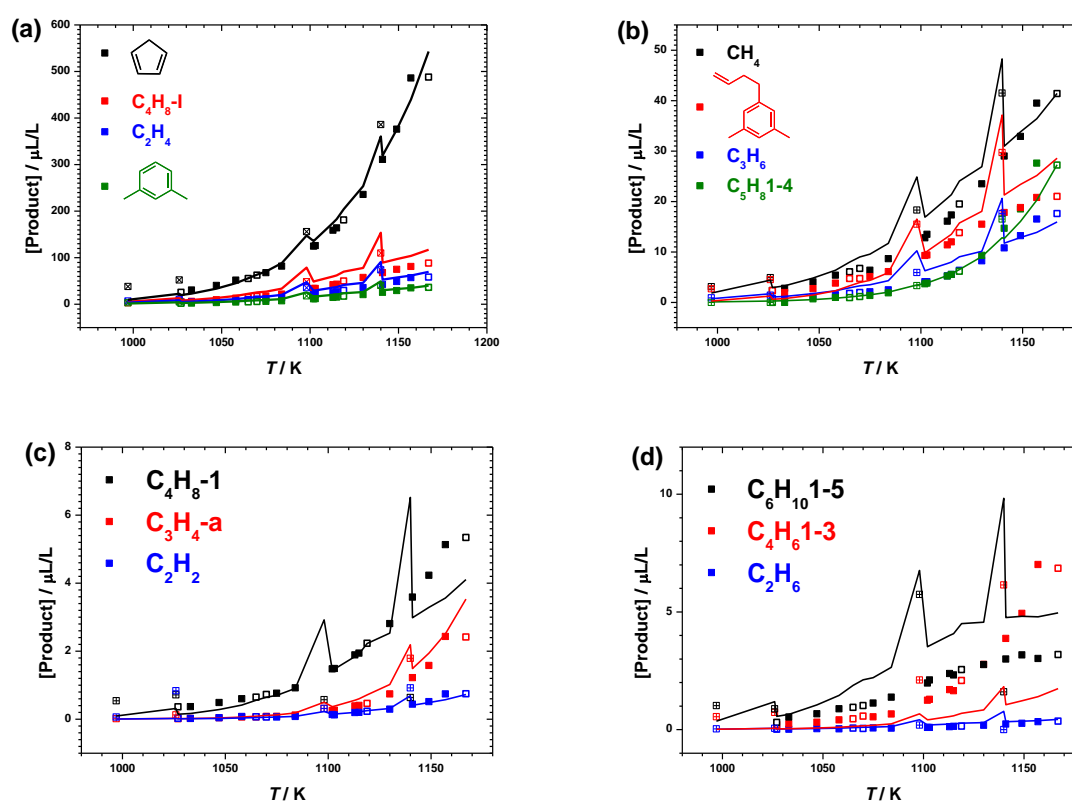


Figure 28. Experimental (symbols)¹⁶ and modelled (lines) concentration profiles for products generated from \dot{H} atom addition to cyclopentene at temperatures over 997–1167 K and pressures at 2.6–3.7 bar. The solid symbols represent results for Mixture A, with open symbols and crossed symbols representing those for Mixture B and Mixture C, respectively.

In addition, the concentration profiles of C₅H₆ (formed via H-atom abstraction reactions of cyC₅H₈ by \dot{H} atoms), D13MB (formed via T135MB + $\dot{H} \rightarrow$ D13MB + $\dot{C}H_3$), 1,4-C₅H₈ (formed via isomerization of cyC₅H₈) are also accurately predicted by our model. The largest deviation between the model and experimental data are observed for 1,3-C₄H₆ (up to a factor of five). The known pathways in our model relating to the formation and consumption of 1,3-

C₄H₆ tend to under-predict [1,3-C₄H₆] and this was also noted in Manion and Awan's studies. Although 1,3-C₄H₆ isn't the main product for cyclopentene + $\dot{\text{H}}$, the chemistry related to its formation and consumption may be important for the other fuels and more studies about its chemistry will be useful for model development. In general, the chemical kinetic model developed in this work can qualitatively and quantitatively predict the concentration profiles of the reactants and important products involved in cyC₅H₁₀/cyC₅H₈ + $\dot{\text{H}}$ systems, which indicates the reliability of our thermochemistry and kinetic calculation results for species and reactions on $\dot{\text{C}}_5\text{H}_9$ PES.

■ Conclusions

Based on the comprehensive study of the $\dot{\text{C}}_5\text{H}_9$ PES in Part I of this study, the calculated high-pressure limiting rate constants, together with the unimolecular decomposition reactions of 1,3-pentadiene, H-atom abstraction reactions of 1,3-, 1,4-C₅H₈, cyC₅H₈ by $\dot{\text{H}}$ atoms, and H-atom abstraction reactions of propene by vinyl radicals, are used to identify the dominant reaction pathways for four systems: 1,3-pentadiene + $\dot{\text{H}}$, 1,4-pentadiene + $\dot{\text{H}}$, cyclopentene + $\dot{\text{H}}$, and vinyl + propene. Based on the important pathways identified from the reaction pathway analysis, a simplified $\dot{\text{C}}_5\text{H}_9$ PES is generated including 18 species and 25 TSs. The SPEs for radicals and TSs on the simplified PES are recalculated at the ROCCSD(T)/aug-cc-pVTZ level of theory with basis set corrections using MP2/aug-cc-pVXZ (where X = T and Q).

Pressure-dependent rate constants are calculated in the temperature range 300–2000 K and at pressures in the range 0.01–100 atm using MESS, with spin-restricted energies used for important species on the simplified $\dot{\text{C}}_5\text{H}_9$ PES and spin-unrestricted energies used for the other species. The reactions on the $\dot{\text{C}}_5\text{H}_9$ PES are classified into unimolecular and bimolecular reactions. For bimolecular reactions (1,3-/1,4-/cyC₅H₈ + $\dot{\text{H}}$, $\dot{\text{C}}_3\text{H}_5\text{-a}$ + C₂H₄, C₃H₆ + $\dot{\text{C}}_2\text{H}_3$), the pressure-dependency of the total addition rate constants and product branching ratios are discussed. The rate constants for H-atom abstraction of these bimolecular reactions are compared with the total addition rate constants. Similarly, the pressure-dependency of the total addition rate constants and product branching ratios are also discussed for important unimolecular reactions. The high-pressure limiting and pressure-dependent rate constants are compared with available literature data with good agreement observed.

A chemical kinetic model is developed in this work with pressure-dependent rate constants for reactions on the $\dot{\text{C}}_5\text{H}_9$ PES using thermochemistry for C₅ species based on AramcoMech 3.0. Secondary chemistry for radical initiators and scavengers used in the

experiment and thermochemistry and kinetic parameters for these species are added to the mechanism to appropriately simulate the literature experiments. This model is used to predict the mole fractions of different products generated for $\dot{\text{H}}$ atom addition to cyclopentane and cyclopentene. The comparisons show that our model is able to reproduce the consumption of the reactants and formation of the main products and can qualitatively and quantitatively predict the concentration profiles measured in the experiments.

Considering the limited literature data for thermochemistry (especially entropy and heat capacities) of C_5H_8 and C_5H_9 species, and the pressure-dependent rate constants for reactions on the $\dot{\text{C}}_5\text{H}_9$ PES, this work is complementary for the development of a comprehensive pyrolysis and oxidation mechanism for C_1 – C_5 hydrocarbons and oxygenated fuels, and higher order alkanes and alkenes for which dienes and aromatics are important intermediates.

Acknowledgements

This study is supported by Science Foundation Ireland and the China Scholarship Council (CSC). The authors want to acknowledge the financial support of Science Foundation Ireland under Grant No. 15/IA/3177 and 16/SP/3829, and the provision of computational resources from ICHEC under the NUI Galway shared condominium accounts. The Computational resources are provided by the Irish Centre for High-End Computing (ICHEC), under project number ngche063c, ngcom006c and ngche058c. The authors are grateful to Stephen Klippenstein for the help with MESS code study. Chong-Wen Zhou acknowledges the support from National Science and Technology Major Project (2017-III-0004-0028) and Beihang University under the Fundamental Research Funds.

Supporting Information

Unimolecular decomposition reactions of 1,3-pentadiene, H-abstraction reactions of 1,4-pentadiene/cyclopentene by $\dot{\text{H}}$ atoms, H-abstraction reactions of propene by vinyl radicals, β -scission reactions of 1,3- $\dot{\text{C}}_5\text{H}_9$ and 1,4- $\dot{\text{C}}_5\text{H}_9$, simplified $\dot{\text{C}}_5\text{H}_9$ PES, species list for $\dot{\text{C}}_5\text{H}_9$ PES, $\dot{\text{C}}_5\text{H}_9$ mechanism including calculated rate constants and thermochemistry, mechanism and input files used for $\text{cyC}_5\text{H}_8/\text{cyC}_5\text{H}_{10} + \dot{\text{H}}$ experimental simulation, and output file of MESS calculation.

Reference

1. Sun, Y.; Zhou, C.-W.; Somers, K. P.; Curran, H. J., Ab Initio/Transition-State Theory Study of the Reactions of $\dot{\text{C}}_5\text{H}_9$ Species of Relevance to 1,3-Pentadiene, Part I: Potential Energy Surfaces, Thermochemistry, and High-Pressure Limiting Rate Constants. *J. Phys. Chem. A* **2019**, *123*, 9019-9052.

2. Georgievskii, Y.; Miller, J. A.; Burke, M. P.; Klippenstein, S. J., Reformulation and Solution of the Master Equation for Multiple-Well Chemical Reactions. *J. Phys. Chem. A* **2013**, *117*, 12146-12154.
3. Georgievskii, Y. *Mess*, S. J. Klippenstein, MESS. 2016.3.23.
4. Tsang, W., Chemical Kinetic Data Base for Combustion Chemistry Part V. Propene. *Journal of Physical and Chemical Reference Data* **1991**, *20*, 221-273.
5. Fahr, A.; Stein, S. In *Reactions of Vinyl and Phenyl Radicals with Ethyne, Ethene and Benzene*, 22nd Symposium (International) on Combustion, Elsevier: 1988; pp 1023-1029.
6. Matheu, D. M.; Green, W. H.; Grenda, J. M., Capturing Pressure-Dependence in Automated Mechanism Generation: Reactions through Cycloalkyl Intermediates. *International Journal of Chemical Kinetics* **2003**, *35*, 95-119.
7. Saeys, M.; Reyniers, M. F.; Marin, G. B.; Van Speybroeck, V.; Waroquier, M., Ab Initio Group Contribution Method for Activation Energies for Radical Additions. *AIChE J.* **2004**, *50*, 426-444.
8. Tsang, W., Mechanism and Rate Constants for the Decomposition of 1-Pentenyl Radicals. *J. Phys. Chem. A* **2006**, *110*, 8501-8509.
9. Sabbe, M. K.; Reyniers, M. F.; Van Speybroeck, V.; Waroquier, M.; Marin, G. B., Carbon - Centered Radical Addition and B - Scission Reactions: Modeling of Activation Energies and Pre - Exponential Factors. *ChemPhysChem* **2008**, *9*, 124-140.
10. Sirjean, B.; Glaude, P.-A.; Ruiz-Lopez, M.; Fournet, R., Theoretical Kinetic Study of Thermal Unimolecular Decomposition of Cyclic Alkyl Radicals. *J. Phys. Chem. A* **2008**, *112*, 11598-11610.
11. Goldsmith, C. F.; Ismail, H.; Abel, P. R.; Green, W. H., Pressure and Temperature Dependence of the Reaction of Vinyl Radical with Alkenes II: Measured Rates and Predicted Product Distributions for Vinyl+Propene. *Proceedings of the Combustion Institute* **2009**, *32*, 139-148.
12. Awan, I. A.; Burgess, D. R.; Tsang, W.; Manion, J. A., Shock Tube Study of the Decomposition of Cyclopentyl Radicals. *Proceedings of the Combustion Institute* **2011**, *33*, 341-349.
13. Wang, K.; Villano, S. M.; Dean, A. M., Reactions of Allylic Radicals That Impact Molecular Weight Growth Kinetics. *Physical Chemistry Chemical Physics* **2015**, *17*, 6255-6273.
14. Wang, K.; Villano, S. M.; Dean, A. M., Reactivity–Structure-Based Rate Estimation Rules for Alkyl Radical H Atom Shift and Alkenyl Radical Cycloaddition Reactions. *J. Phys. Chem. A* **2015**, *119*, 7205-7221.
15. Al Rashidi, M. J.; Thion, S.; Togbé, C.; Dayma, G.; Mehl, M.; Dagaut, P.; Pitz, W. J.; Zádor, J.; Sarathy, S. M., Elucidating Reactivity Regimes in Cyclopentane Oxidation: Jet Stirred Reactor Experiments, Computational Chemistry, and Kinetic Modeling. *Proceedings of the Combustion Institute* **2017**, *36*, 469-477.
16. Manion, J. A.; Awan, I. A., A Shock Tube Study of H Atom Addition to Cyclopentene. *International Journal of Chemical Kinetics* **2018**, *50*, 225-242.
17. Gordon, A. S., A Study of Some Reactions of the Cyclopentyl Radical. *Canadian Journal of Chemistry* **1965**, *43*, 570-581.
18. Getty, R. R., J. A. Kerr, and A. F. Trotman-Dickenson, The Reactions of Alkyl Radicals. Part XII. The Additions of Methyl, Ethyl, and Isopropyl Radicals to Allene. *Journal of the Chemical Society A* **1967**, 979-982.
19. Watkins, K.; Olsen, D., Cyclization and Decomposition of 4-Penten-1-Yl Radicals in the Gas Phase. *The Journal of Physical Chemistry* **1972**, *76*, 1089-1092.
20. Stein, S.; Rabinovitch, B., Ring Opening and Isomerization of a Series of Chemically Activated Cycloalkyl Radicals. *The Journal of Physical Chemistry* **1975**, *79*, 191-198.

21. Baldwin, R.; Walker, R. In *Elementary Reactions in the Oxidation of Alkenes*, Symposium (International) on Combustion, Elsevier: 1981; pp 819-829.
22. Gierczak, T.; Gawłowski, J.; Niedzielski, J., Mutual Isomerization of Cyclopentyl and 1 - Penten - 5 - Y1 Radicals. *International journal of chemical kinetics* **1986**, *18*, 623-637.
23. Kopinke, F. D., G. Zimmermann, G. Bach, B. Ondruschka., Pyrolysis of [5 - ¹⁴c] - 1 - Pentene - Evidence for Homoallylic Rearrangements at 873 K. *International journal of chemical kinetics* **1986**, *18*, 159-163.
24. Perrin, D.; Richard, C.; Martin, R., H₂s - Promoted Thermal Isomerization of Cis - 2 - Pentene to 1 - Pentene and Trans - 2 - Pentene around 800 K. *International journal of chemical kinetics* **1988**, *20*, 621-632.
25. Tsang, W.; Walker, J. A., Pyrolysis of 1, 7-Octadiene and the Kinetic and Thermodynamic Stability of Allyl and 4-Pentenyl Radicals. *The Journal of Physical Chemistry* **1992**, *96*, 8378-8384.
26. Handford-Styring, S. M.; Walker, R. W., Addition of Cyclopentane to Slowly Reacting Mixtures of H₂+ O₂ between 673 and 783 K: Reactions of H and Oh with Cyclopentane and of Cyclopentyl Radicals. *Journal of the Chemical Society, Faraday Transactions* **1995**, *91*, 1431-1438.
27. Clarke, J. S.; Donahue, N. M.; Kroll, J. H.; Rypkema, H. A.; Anderson, J. G., An Experimental Method for Testing Reactivity Models: A High-Pressure Discharge- Flow Study of H+ Alkene and Haloalkene Reactions. *J. Phys. Chem. A* **2000**, *104*, 5254-5264.
28. Li, Y.; Zhou, C.-W.; Somers, K. P.; Zhang, K.; Curran, H. J., The Oxidation of 2-Butene: A High Pressure Ignition Delay, Kinetic Modeling Study and Reactivity Comparison with Isobutene and 1-Butene. *Proceedings of the Combustion Institute* **2017**, *36*, 403-411.
29. Zhou, C.-W., et al., A Comprehensive Experimental and Modeling Study of Isobutene Oxidation. *Combust. Flame* **2016**, *167*, 353-379.
30. Burke, U.; Metcalfe, W. K.; Burke, S. M.; Heufer, K. A.; Dagaut, P.; Curran, H. J., A Detailed Chemical Kinetic Modeling, Ignition Delay Time and Jet-Stirred Reactor Study of Methanol Oxidation. *Combust. Flame* **2016**, *165*, 125-136.
31. Burke, S. M., et al., An Experimental and Modeling Study of Propene Oxidation. Part 2: Ignition Delay Time and Flame Speed Measurements. *Combust. Flame* **2015**, *162*, 296-314.
32. Burke, S. M.; Metcalfe, W.; Herbinet, O.; Battin-Leclerc, F.; Haas, F. M.; Santner, J.; Dryer, F. L.; Curran, H. J., An Experimental and Modeling Study of Propene Oxidation. Part 1: Speciation Measurements in Jet-Stirred and Flow Reactors. *Combust. Flame* **2014**, *161*, 2765-2784.
33. Metcalfe, W. K.; Burke, S. M.; Ahmed, S. S.; Curran, H. J., A Hierarchical and Comparative Kinetic Modeling Study of C1- C2 Hydrocarbon and Oxygenated Fuels. *International Journal of Chemical Kinetics* **2013**, *45*, 638-675.
34. Kéromnès, A., et al., An Experimental and Detailed Chemical Kinetic Modeling Study of Hydrogen and Syngas Mixture Oxidation at Elevated Pressures. *Combust. Flame* **2013**, *160*, 995-1011.
35. Zhou, C.-W.; Li, Y.; Burke, U.; Banyon, C.; Somers, K. P.; Ding, S.; Khan, S.; Hargis, J. W.; Sikes, T.; Mathieu, O., An Experimental and Chemical Kinetic Modeling Study of 1, 3-Butadiene Combustion: Ignition Delay Time and Laminar Flame Speed Measurements. *Combust. Flame* **2018**, *197*, 423-438.
36. *Ansys Chemkin-Pro 15131, Reaction Design: San Diego*, ANSYS CHEMKIN-PRO 15131, Reaction Design: San Diego, 2013.
37. Binkley, J.; Pople, J.; Dobosh, P., The Calculation of Spin-Restricted Single-Determinant Wavefunctions. *Molecular Physics* **1974**, *28*, 1423-1429.

38. Crawford, T. D.; Lee, T. J.; Schaefer III, H. F., A New Spin-Restricted Triple Excitation Correction for Coupled Cluster Theory. *The Journal of chemical physics* **1997**, *107*, 7943-7950.
39. Pople, J. A.; Head - Gordon, M.; Raghavachari, K., Quadratic Configuration Interaction. A General Technique for Determining Electron Correlation Energies. *The Journal of chemical physics* **1987**, *87*, 5968-5975.
40. Martin, J. M., Ab Initio Total Atomization Energies of Small Molecules—Towards the Basis Set Limit. *Chemical physics letters* **1996**, *259*, 669-678.
41. Cagnina, S.; Nicolle, A.; de Bruin, T.; Georgievskii, Y.; Klippenstein, S. J., First-Principles Chemical Kinetic Modeling of Methyl Trans-3-Hexenoate Epoxidation by Ho₂. *J. Phys. Chem. A* **2017**, *121*, 1909-1915.
42. Al Rashidi, M. J.; Mehl, M.; Pitz, W. J.; Mohamed, S.; Sarathy, S. M., Cyclopentane Combustion Chemistry. Part I: Mechanism Development and Computational Kinetics. *Combustion and Flame* **2017**, *183*, 358-371.
43. Li, Y.; Klippenstein, S. J.; Zhou, C.-W.; Curran, H. J., Theoretical Kinetics Analysis for H Atom Addition to 1, 3-Butadiene and Related Reactions on the C₄H₇ Potential Energy Surface. *J. Phys. Chem. A* **2017**, *121*, 7433-7445.
44. Klippenstein, S. J., From Theoretical Reaction Dynamics to Chemical Modeling of Combustion. *Proceedings of the Combustion Institute* **2017**, *36*, 77-111.
45. Brown, N. J.; Bastien, L. A.; Price, P. N., Transport Properties for Combustion Modeling. *Progress in Energy and Combustion Science* **2011**, *37*, 565-582.
46. Jasper, A. W.; Miller, J. A., Lennard-Jones Parameters for Combustion and Chemical Kinetics Modeling from Full-Dimensional Intermolecular Potentials. *Combust. Flame* **2014**, *161*, 101-110.
47. Pfaendtner, J.; Yu, X.; Broadbelt, L. J., The 1-D Hindered Rotor Approximation. *Theoretical Chemistry Accounts* **2007**, *118*, 881.
48. Eckart, C., The Penetration of a Potential Barrier by Electrons. *Physical Review* **1930**, *35*, 1303.
49. Somers, K. P., On the Pyrolysis and Combustion of Furans: Quantum Chemical, Statistical Rate Theory, and Chemical Kinetic Modelling Studies. Curran, H. J.; Science Foundation, I., Eds. 2014.
50. Dean, A., Predictions of Pressure and Temperature Effects Upon Radical Addition and Recombination Reactions. *The Journal of Physical Chemistry* **1985**, *89*, 4600-4608.
51. Chang, A.; Bozzelli, J.; Dean, A., Kinetic Analysis of Complex Chemical Activation and Unimolecular Dissociation Reactions Using Qrrk Theory and the Modified Strong Collision Approximation. *Zeitschrift für Physikalische Chemie* **2000**, *214*, 1533.
52. Power, J.; Somers, K. P.; Zhou, C.-W.; Peukert, S.; Curran, H. J., Theoretical, Experimental, and Modeling Study of the Reaction of Hydrogen Atoms with 1-and 2-Pentene. *J. Phys. Chem. A* **2019**, *123*, 8506-8526.
53. Awan, I. A.; Burgess Jr, D. R.; Manion, J. A., Pressure Dependence and Branching Ratios in the Decomposition of 1-Pentyl Radicals: Shock Tube Experiments and Master Equation Modeling. *J. Phys. Chem. A* **2012**, *116*, 2895-2910.
54. Al Rashidi, M. J.; Mármol, J. C.; Banyon, C.; Sajid, M. B.; Mehl, M.; Pitz, W. J.; Mohamed, S.; Alfazazi, A.; Lu, T.; Curran, H. J., Cyclopentane Combustion. Part II. Ignition Delay Measurements and Mechanism Validation. *Combust. Flame* **2017**, *183*, 372-385.
55. Liu, Y.-X.; Tian, Z.-Y., Oxidation Chemistry of Four C₉H₁₂ Isomeric Transportation Fuels: Experimental and Modeling Studies. *Combust. Flame* **2019**, *205*, 165-179.
56. Ritter, E. R.; Bozzelli, J. W., Therm: Thermodynamic Property Estimation for Gas Phase Radicals and Molecules. *International Journal of Chemical Kinetics* **1991**, *23*, 767-778.

57. Klippenstein, S. J.; Cavallotti, C., Ab Initio Kinetics for Pyrolysis and Combustion Systems. In *Computer Aided Chemical Engineering*, Elsevier: 2019; Vol. 45, pp 115-167.
58. Miller, J. A.; Klippenstein, S. J., Determining Phenomenological Rate Coefficients from a Time-Dependent, Multiple-Well Master Equation: "Species Reduction" at High Temperatures. *Physical Chemistry Chemical Physics* **2013**, *15*, 4744-4753.
59. Zhang, P.; Klippenstein, S. J.; Law, C. K., Ab Initio Kinetics for the Decomposition of Hydroxybutyl and Butoxy Radicals of N-Butanol. *J. Phys. Chem. A* **2013**, *117*, 1890-1906.
60. Sarathy, S. M.; Westbrook, C. K.; Mehl, M.; Pitz, W. J.; Togbe, C.; Dagaut, P.; Wang, H.; Oehlschlaeger, M. A.; Niemann, U.; Seshadri, K., Comprehensive Chemical Kinetic Modeling of the Oxidation of 2-Methylalkanes from C7 to C20. *Combust. Flame* **2011**, *158*, 2338-2357.
61. Goldsmith, C. F.; Ismail, H.; Green, W. H., Pressure and Temperature Dependence of the Reaction of Vinyl Radical with Alkenes Iii: Measured Rates and Predicted Product Distributions for Vinyl + Butene. *J. Phys. Chem. A* **2009**, *113*, 13357-13371.
62. Ismail, H.; Goldsmith, C. F.; Abel, P. R.; Howe, P.-T.; Fahr, A.; Halpern, J. B.; Jusinski, L. E.; Georgievskii, Y.; Taatjes, C. A.; Green, W. H., Pressure and Temperature Dependence of the Reaction of Vinyl Radical with Ethylene. *J. Phys. Chem. A* **2007**, *111*, 6843-6851.
63. Barker, J. R., Multiple - Well, Multiple - Path Unimolecular Reaction Systems. I. Multiwell Computer Program Suite. *International Journal of Chemical Kinetics* **2001**, *33*, 232-245.
64. J. R. Barker, T. L. N., J. F. Stanton, C. Aieta, M. Ceotto, F. Gabas, T. J. D. Kumar, C. G. L. Li, L. L. Lohr, A. Maranzana, N. F. Ortiz, J. M. Preses, J. M. Simmie, J. A. Sonk, P. J. Stimac *Multiwell-2017 Software Suite*, University of Michigan: Ann Arbor: Michigan, USA, 2017.
65. Barker, J. R., Energy Transfer in Master Equation Simulations: A New Approach. *International Journal of Chemical Kinetics* **2009**, *41*, 748-763.
66. Atkins, P.; De Paula, J., *Elements of Physical Chemistry*; Oxford University Press, USA, 2013.
67. Bugler, J.; Power, J.; Curran, H. J., A Theoretical Study of Cyclic Ether Formation Reactions. *Proceedings of the Combustion Institute* **2017**, *36*, 161-167.
68. Jasper, A. W.; Hansen, N., Hydrogen-Assisted Isomerizations of Fulvene to Benzene and of Larger Cyclic Aromatic Hydrocarbons. *Proceedings of the Combustion Institute* **2013**, *34*, 279-287.
69. Jasper, A. W.; Gruy, Z. B.; Harding, L. B.; Georgievskii, Y.; Klippenstein, S. J.; Wagner, A. F., Anharmonic Rovibrational Partition Functions for Fluxional Species at High Temperatures Via Monte Carlo Phase Space Integrals. *J. Phys. Chem. A* **2018**.